cloned into a pCI mammalian expression vector (Promega, Madison, WI) that had been digested with the same restriction enzymes. The construct of Flag-hADAR2 was amplified using PCR with primers specific for Flag-ADAR2UP1 (5′-AAAAAGCTAGCTCCACCATGGATTACAAG-GATGACGACGATAAGATCGATATAGAAGATGAAG-3′) and Flag-ADAR2DW1 (5′-AAAAAGGTACCTCAGGGCGTGAGTGAGAAC-3′). The resultant products were digested with *Nhe*I and *Kpn*I and cloned into pCI (Promega). Site-directed mutagenesis of hADAR2 was conducted to substitute Ala for Glu (E396A) using a KOD Plus mutagenesis kit (Toyobo, Japan). All constructs were verified by DNA sequencing.

### Cell culture and transfection

Neuro2a cells were cultured in DMEM high-glucose medium (WAKO, Tokyo, Japan) supplemented with 10% foetal bovine serum (Invitrogen, Carlsbad, CA, USA), 100 U/ml penicillin and 100 μg/ml streptomycin (Invitrogen) in 5% $CO_2$ at 37°C. The culture medium was changed once after 24 h and then every 2 days. The cells were grown in 6-well plates at a density of $3.5 \times 10^4$ cell/cm$^2$. The cultured cells were transfected with 2.5 μg of expression plasmid using Lipofectamine LTX and PLUS™ reagents (Invitrogen). The cells were cultured for 72 h and then harvested.

### Production of recombinant AAV vectors

The AAV vector plasmids contained an expression cassette consisting of the mouse synapsin I (SYNI) promoter, followed by the cDNA of interest, a woodchuck hepatitis virus posttranscriptional regulatory element, and a simian virus 40 polyadenylation signal sequence between the inverted terminal repeats of the AAV3 genome. The AAV9 vp cDNA was synthesized, and the sequence was identical to that previously described (Gao et al, 2004) except for the substitution of thymidine for adenine 1337, which introduced an amino acid change from tyrosine to phenylalanine at position 446 (Petrs-Silva et al, 2011). Recombinant AAV vectors were produced by transient transfection of HEK293 cells using the vector plasmid, an AAV3 rep and AAV9 vp expression plasmid, and the adenoviral helper plasmid pHelper (Agilent Technologies, Santa Clara, CA) as described previously (Li et al, 2006). The recombinant viruses were purified by isolation from two sequential continuous CsCl gradients, and the viral titres were determined by qRT-PCR. The viral vectors used for expression of hADAR2 (AAV9-hADAR2), an inactive mutant hADAR2 with an E396A amino acid substitution (AAV9-hADAR2$^{E396A}$), Flag-tagged hADAR2 (AAV9-Flag-hADAR2 and AAV9-Flag-hADAR2$^{E396A}$) and green fluorescent protein (AAV9-GFP), contained the entire cDNA sequences of *ADARB1* (GenBank accession number NM_015833 and NM_015834) or *EGfp*.

### Animals

The animals used in this study were homozygous conditional ADAR2 knockout mice (*ADAR2*$^{flox/flox}$/VAChT-Cre.Fast; AR2). In AR2 mice, *Adarb1* encoding ADAR2 is conditionally targeted in motor neurons using the Cre/loxP system, and ADAR2 activity is completely ablated in approximately 50% of motor neurons, which are therefore unable to edit the Q/R site of GluA2. AR2 mice display slowly progressing motor dysfunction resulting from a loss of spinal AHCs. Because reduced GluA2 Q/R site-editing occurs in motor neurons in sporadic ALS, AR2 mice recapitulate the molecular pathology of sporadic ALS.

Recombinant AAV vectors were injected intravenously into mice via the mouse tail vein. In some experiments (Supporting Information Fig S4), AAV vectors were injected in the left ventricle of the heart of mice anaesthetized with pentobarbital (50 mg/kg, i.p.) over a period of 1 min with a 0.5 ml syringe equipped with a 29-gauge needle. Homozygous AR2 mice ($n = 16$) were injected with AAV9-hADAR2 vectors ($2.14 \times 10^{12}$ vg/body) before ($n = 11$) or after ($n = 5$) the initiation of motor dysfunction that was defined by a decline in rotarod performance. Age-adjusted AR2 mice were used as disease controls, and WT or Cre-negative ADAR2$^{flox}$ mice of the same strain were used as normal controls. All studies were performed in accordance with the Guidelines for Animal Studies of the University of Tokyo and NIH. The Committee on Animal Handling at the University of Tokyo also approved the experimental procedures. AR2 mice injected with AAV9-hADAR2 vectors before the initiation of motor dysfunction were used for immunohistochemistry and biochemical analyses at 36 weeks of age ($n = 5$–8). In some experiments, WT mice of the same strain at 10 weeks of age was injected with AAV9-GFP ($7.2 \times 10^{11}$ vg/body) and histologically observed 11 weeks after the injection.

### Behavioural analyses

We determined the maximal time before falling in a mouse-specific rotarod (Muromachi Kikai Co. LTD MK-610A). After training at 10 rpm, mice were placed on the rotarod turning at a speed of 4 rpm, and the speed of the rotarod was then accelerated to 40 rpm linearly over 120 s. Each run consisted of three trials, and the maximum value of the three runs was recorded. We defined disease onset as the time point at which the mice exhibited <75% of the average performance of the initial 3 weeks for three consecutive trials. The end point was set as the point at which the falling time was <10 s for 3 consecutive weeks or the mice reached 36 weeks of age. Grip power was measured using a dynamometer (NS-TRM-M; Neuroscience Corp.). Spontaneous activity data from individual mice were collected using a piezoelectric sensor sheet (Biotex) as previously reported by Nakamura et al (2008). Mice were housed in cages on a 12 h:12 h light-dark cycle with free access to food and water. Piezoelectric sensor sheets placed under the cages for 24 h were used to measure the daily activity of the mice. The sensor sheets' output voltage signals were proportional to the pressure generated by the activity of the mice. The signals were sampled at 100 Hz with 16-bit resolution after passing through a 0.5–50 Hz band-pass filter and then digitized and stored on a computer every minute. To evaluate spontaneous activity, we calculated the average of 24 h of data and recorded this value. All behavioural measurements were conducted weekly by a researcher, who was blind to the virus administration condition, genotype and age of the mice.

### Western blot analysis

Neuro2a cells and frozen tissues were homogenized by sonication in 20 volumes of extraction buffer (50 mM HEPES, pH 7.5, 1 mM EDTA, 100 mM NaCl, 10 mM DTT and 0.1% CHAPS). The homogenate was centrifuged at 1000 g for 10 min at 4°C. The supernatant was boiled with 4 × SDS gel loading buffer and subjected to SDS–PAGE. After electrophoresis, proteins were transferred to an Immobilon-P transfer membrane (Millipore, Bedford, MA), and immunoblotting for ADAR2, Flag and beta-actin was conducted. Goat anti-ADAR2 (E-20) (Santa Cruz Biotech.) (1:2000), rabbit anti-DYKDDDDK Tag (Flag) (Cell Signaling Technology) (1:2000), and rabbit anti-beta-actin (IMGENEX Corp.) (1:2000) were used as primary antibodies, and peroxidase-conjugated goat anti-rabbit IgG (Cell Signaling Technology, Inc.) (1:2000) and

## The paper explained

### PROBLEM:

ALS is the most common adult-onset motor neuron disease in which motor neurons innervating skeletal muscles selectively and progressively undergo degeneration from undetermined mechanism. The progressive nature of the disease leads the patients with ALS to death from failure of respiratory muscles within a few years of onset without effective therapy. Recently, with the progress of pathogenic mechanism of ALS, several potential target molecules for therapy have been demonstrated. However, because motor neurons are localized widely in the nuclei of cranial motor nerves and the spinal cord, global delivery of therapeutic agents to the motor neurons is required to accomplish therapeutic effects. Although delivery of the therapeutic agents through the vasculature enables widespread delivery, the blood–brain-barrier prevents entrance of molecules from blood to the brain and spinal cord. Therefore, safe delivery of therapeutic agents widely to motor neurons using appropriate vehicles is required for development of ALS therapy.

### RESULTS:

Progressive death of the motor neurons in the brains and spinal cords cause ALS phenotype and expression of abnormal GluA2 (a subunit of the AMPA receptor that is involved in the neuronal excitation in the brain and spinal cord) with glutamine residue at the glutamine/arginine (Q/R) site (GluA2Q) is a disease-specific and potentially death-causing molecular abnormality occurring in the motor neurons of the patients with sporadic form of ALS that accounts for the majority of ALS patients. Motor neurons normally express $Ca^{2+}$-impermeable AMPA receptors containing GluA2 with arginine residue at the Q/R site (GluA2R) in the assembly, but express $Ca^{2+}$-permeable AMPA receptors when GluA2Q is expressed, which leads motor neurons to death. Given that this event would be closely relevant to ALS etiology, we attempt to develop a therapeutic strategy for ALS by broadly delivering cDNA of ADAR2, the enzyme that converges GluA2Q to GluA2R, to motor neurons in the aim to enhance the expression of normal GluA2R. To achieve widespread and selective expression of the *ADAR2* gene in motor neurons through a peripheral route avoiding off-target delivery, we used a viral vector AAV9 and the neuron-specific SYN1 promoter. A single intravenous injection of AAV9-ADAR2 in AR2 mice, which comprise a mechanistic mouse model of sporadic ALS, effectively prevented progressive motor dysfunction and death of motor neurons by enhancing ADAR2 activity. Notably, AAV9-ADAR2 normalized the abnormal expression profile of TDP-43, which is the ALS-specific pathological change, in the remaining motor neurons. Thus, our therapeutic strategy semi-permanently normalized disease phenotype, neuronal death and the disease-specific molecular marker in the ALS model mice.

### IMPACT:

This is the first report on successful pre-clinical ALS therapy based on plausible pathogenic mechanism, achieving semi-permanent therapeutic effects on a mechanistic disease mouse model. Potency of the therapy on the model mice and safety as demonstrated by the clinical use in some other diseases provide delivery of the *ADAR2* gene using AAV9 with SYN1 promoter as potential therapy applicable to patients with ALS. Intravenous route of delivery using a relatively safe vehicle would facilitate clinical trials.

peroxidase-conjugated affinipure donkey anti-goat IgG (H + L) (Jackson ImmunoResearch, West Grove, PA) (1:2000) were used as secondary antibodies. Visualization was conducted using ECL plus Western blotting detection reagents (GE Healthcare Bioscience, Piscataway, NJ, USA). Specific bands were detected using a LAS 3000 system (Fujifilm, Tokyo).

#### RNA extraction and reverse transcription

Total RNA was isolated from the cells and spinal cords of mice using an RNeasy micro kit (Qiagen) and trizol (Invitrogen) and treated with DNaseI as recommended by the manufacturer. First-strand cDNA was synthesized from the total RNA using a Onestep RT-PCR kit (Qiagen), Ready-To-Go You-Prime First-Strand Beads (GE Healthcare Bioscience) and 50 ng of random primers (Invitrogen) as recommended by the manufacturer.

#### Analysis of the conversion of adenosine to inosine at the GluA2 Q/R site and CYFIP2 K/E site editing

The efficiency of the conversion of adenosine to inosine in the GluA2 mRNA, pre-mRNA and the CYFIP2 mRNA was calculated using a Bioanalyzer 2100 (Agilent Technologies) following the digestion of PCR products with restriction enzymes (Bhalla et al, 2004; Kawahara et al, 2003, 2004). The amplified GluA2 mRNA and pre-mRNA PCR products were digested with *Bbv*I (New England Biolabs, Ipswich, MA). The amplified CYFIP2 mRNA PCR products were digested with *Mse*I (New England Biolabs).

The PCR products from edited GluA2 pre-mRNA molecules contain one intrinsic *Bbv*I recognition site, whereas the products originating from the unedited GluA2 contain an additional recognition site. Therefore, digestion of the PCR products from the edited GluA2 pre-mRNA and GluA2 mRNA should produce two bands (129 and 71 bp, pre-mRNA; 200 and 44 bp, mRNA), whereas digestion of bands originating from the unedited GluA2 pre-mRNA or mRNA molecules should produce three bands (91, 38 and 71 bp, pre-mRNA; 119, 44 and 81 bp, mRNA). The density of the 71- or 44-bp band, which results from digestion of both the edited and unedited pre-mRNA or mRNA, and the 129- or 200-bp band, which is solely the product of the edited pre-mRNA or mRNA, were quantified and the editing efficiency was calculated as the ratio of former to the latter for each sample (Nishimoto et al, 2008; Sawada et al, 2009). Similarly, *Mse*I digestion of the RT-PCR product generated from edited CYFIP2 yields two bands (117 and 209 bp), whereas that generated from unedited CYFIP2

mRNA yields three bands (117, 60 and 149 bp) (Nishimoto et al, 2008). The PCR primers used in these assays are provided in Supporting Information Table S1.

### Real-time quantitative polymerase chain reaction

Quantitative PCR was performed using a LightCycler System (Roche Diagnostics, Indianapolis, IN). Standards and cDNA samples were amplified in a reaction mixture (20 μl total volume) composed of 10 μl of 2× LightCycler 480 Probes Master Roche (Roche Diagnostics), each primer at 0.5 μM and the Universal Probe Library (Roche Diagnostics) at 0.1 μM. We determined the expression level of ADAR2 mRNA using different primer pairs for mouse ADAR2, human ADAR2 and total (both human and mouse) ADAR2 cDNA (Supporting Information Table S2). The reaction was initially incubated at 95°C for 10 min, and amplification of the templates was performed with a denaturing step at 95°C for 10 s and a primer annealing step at 60°C for 30 s. As an internal control, the expression of human β-actin was also measured in each sample using a LightCycler Primer/Probe Set (Roche Diagnostics; Supporting Information Table S2) and the same PCR conditions (Sawada et al, 2009; Yamashita et al, 2012c).

### Immunohistochemistry

Under deep anesthesia with isoflurane mice, were transcardially perfused with 3.5% paraformaldehyde and 0.5% glutaraldehyde in phosphate-buffered saline (PBS). The brains and spinal cords were removed and immersed in serially increasing concentrations of sucrose–PBS solutions (final sucrose concentration of 30%). The sucrose-immersed spinal cords were cut at a thickness of 10 μm with a cryostat (Model LEICA CM1850; Leica). The sections were immunostained with a standard avidin–biotin–immunoperoxidase complex method using VECTASTAIN ABC IgGs (Vector Co.) for the secondary antibodies. Rabbit anti-TDP-43 (ProteinTech Group, Inc., 1:100) and sheep anti-rat RED1 (ADAR2; Exalpha Biologicals, Inc., 1:100) were used for the primary antibodies. Colour was developed using the HRP-DAB System (Vector Co.).

Immunofluorescent staining of the sections was performed using rabbit anti-TDP-43 (ProteinTech Group, Inc., 1:200) and sheep anti-rat RED1 (ADAR2; Exalpha Biologicals, Inc., 1:200) as the primary antibodies. Sections were then incubated with Alexa Fluor 555 donkey anti-sheep IgG (Invitrogen, 1:200) and Alexa Fluor 488 chicken anti-rabbit IgG (Invitrogen, 1:200), respectively, as the secondary antibodies. The sections were examined under an LSM-510 confocal microscope (Zeiss) after nuclear staining with 0.5 μM TO-PRO-3 for 30 min.

### Morphological observation

Mice were killed by overdose of isoflurane, and the brains and spinal cords were removed and then either quickly frozen on dry ice (right hemisphere and the first cervical to the second lumbar spinal cord segments) or fixed with 3.5% paraformaldehyde and 1% glutaraldehyde in PBS (left hemisphere and the rest of the spinal cord). Frozen samples were stored at −80°C until use. Paraformaldehyde-fixed samples were immersed in the same fixative overnight and then rinsed in PBS. Sections of the fixed fifth lumbar (L5) spinal cord segment were sequentially immunostained for Flag (Flag-hADAR2) and TDP-43 using the immunofluorescence system. The fluorescent images were analysed using a fluorescence microscope (BIOREVO BZ-9000; Keyence Corp, Osaka, Japan). Large AHCs with diameters larger than 20 μm were separately counted for each mouse. TDP-43-positive AHCs (in the ventral grey matter ventral to the line running though the ventral edge of the central canal) were counted in four L5 sections for each mouse. The ventral roots of L5 were then postfixed in 1% phosphate-buffered osmium tetroxide. The signal intensity of TDP-43 was examined using Image J software. TDP-43-positive AHCs were counted when the signal intensity was more than threefold higher than the background. After three washes with phosphate buffer, each sample was dehydrated in a graded series of ethanol and embedded in Epon (Wako). Thin sections (1 μm) of the L5 ventral root were stained with 0.1% toluidine blue, digitized using a BIOREVO BZ-9000 (Keyence), and axons were counted manually by a researcher who was blind to the virus injection condition.

### Tyramide signal amplification (TSA)

The perfusion-fixed, sucrose-immersed spinal cords were cut to a thickness of 12 μm using a cryostat (Model LEICA CM1850; Leica). The sections were incubated with 3.0% $H_2O_2$ in PBS and TNB blocking buffer [0.1 M Tris–HCl, pH 7.5, 0.15M NaCl and 0.5% blocking Reagent (PerkinElmer)]. Sections were serially incubated with goat anti-choline acetyltransferase (ChAT) (Millipore; 1:2000 in TNB blocjing buffer) at 4° C overnight, incubated with HRP-conjugated donkey anti-goat IgG (Abcam, 1:2000) for another 1 h at room temperature and finally incubated with tetramethylrhodamine plus amplification tyramide reagent (1:250 in amplification solution) for 20 min at room temperature. After washing, the sections were subjected to the next round of immunohistochemistry after blocking with 3.0% $H_2O_2$ in PBS. The sections were incubated with the rabbit anti-Flag antibody (Cell Signaling Tech; 1:200) in Can Get Signal buffer A (Toyobo) at 4°C overnight and then serially with HRP-conjugated chicken anti-rabbit IgG (Abcam, 1:2000) in Can Get Signal buffer A (Toyobo) for another 1 h at room temperature and with fluorescein plus amplification tyramide reagent (1:250 in amplification solution) for 20 min at room temperature. The sections were examined under a BIOREVO BZ-9000 microscope (Keyence Corp, Osaka, Japan) after nuclear staining with 0.5 μM TO-PRO-3 for 60 min. Bars represent 50 or 20 μm.

### Statistical analysis

Average data are presented as means and s.e.m. Statistical analyses were conducted using JMP 9 software (SAS Institute, Inc.). For statistical comparisons of two groups, we used unpaired, two-tailed Student's *t* tests or Mann–Whitney *U* tests. Differences were considered significant when $p < 0.05$.

## Author contributions

SK supervised the entire project. TY, KS, SM and SK conceived and designed the experiments. TY, HLC, SM and SK wrote the main text, and TY and HLC made the figures. TY, HLC, STe, KS and SM conducted the experiments and analysed the data. KS and SM generated the AAV9 constructs and virus for the studies. All of the co-authors (TY, HLC, STe, STs, KS, SM and SK) discussed the results and commented on the manuscript.

## Acknowledgements

We thank Naomi Takino, Hitomi Miyauchi, Keiko Ayabe (Jichi Med. Univ.), Kosuke Hachiga, Saori Kaneko and Ai Ono (Tokyo

Univ.) for technical assistance and Prof. Kazunori Kataoka (Univ. Tokyo) for kindly providing us with research facilities. This study was supported in part by a grant-in-aid for scientific research from the Ministry of Health, Labour, and Welfare of Japan to SK (H21-Kokoro-017), grants-in-aid for scientific research from the Japan Society for the Promotion of Science to SK (19390235, 22390173) and to SM (23590473), a grant-in-aid for scientific research on innovative areas (Synapse Neurocircuit Pathology) from the Ministry of Education, Culture, Sports, Science and Technology of Japan to SK and SM, and a grant-in-aid from the research committee of CNS degenerative diseases to SM.

Supporting Information is available at EMBO Molecular Medicine online.

The authors declare that they have no conflict of interest.

## References

Aizawa H, Sawada J, Hideyama T, Yamashita T, Katayama T, Hasebe N, Kimura T, Yahara O, Kwak S (2010) TDP-43 pathology in sporadic ALS occurs in motor neurons lacking the RNA editing enzyme ADAR2. Acta Neuropathol 120: 75-84

Arai T, Hasegawa M, Akiyama H, Ikeda K, Nonaka T, Mori H, Mann D, Tsuchiya K, Yoshida M, Hashizume Y *et al* (2006) TDP-43 is a component of ubiquitin-positive tau-negative inclusions in frontotemporal lobar degeneration and amyotrophic lateral sclerosis. Biochem Biophys Res Commun 351: 602-611

Benkhelifa-Ziyyat S, Besse A, Roda M, Duque S, Astord S, Carcenac R, Marais T, Barkats M (2013) Intramuscular scAAV9-SMN injection mediates widespread gene delivery to the spinal cord and decreases disease severity in SMA mice. Mol Ther 21: 282-290

Bhalla T, Rosenthal JJ, Holmgren M, Reenan R (2004) Control of human potassium channel inactivation by editing of a small mRNA hairpin. Nat Struct Mol Biol 11: 950-956

Dayton RD, Wang DB, Klein RL (2012) The advent of AAV9 expands applications for brain and spinal cord gene delivery. Expert Opin Biol Ther 12: 757-766

Duque S, Joussemet B, Riviere C, Marais T, Dubreil L, Douar AM, Fyfe J, Moullier P, Colle MA, Barkats M (2009) Intravenous administration of self-complementary AAV9 enables transgene delivery to adult motor neurons. Mol Ther 17: 1187-1196

Foust KD, Nurre E, Montgomery CL, Hernandez A, Chan CM, Kaspar BK (2009) Intravascular AAV9 preferentially targets neonatal neurons and adult astrocytes. Nat Biotechnol 27: 59-65

Gao G, Vandenberghe LH, Alvira MR, Lu Y, Calcedo R, Zhou X, Wilson JM (2004) Clades of adeno-associated viruses are widely disseminated in human tissues. J Virol 78: 6381-6388

Hideyama T, Kwak S (2011) When does ALS start? ADAR2-GluA2 hypothesis for the etiology of sporadic ALS. Front Mol Neurosci 4: 33

Hideyama T, Yamashita T, Aizawa H, Tsuji S, Kakita A, Takahashi H, Kwak S (2012) Profound downregulation of the RNA editing enzyme ADAR2 in ALS spinal motor neurons. Neurobiol Dis 45: 1121-1128

Hideyama T, Yamashita T, Suzuki T, Tsuji S, Higuchi M, Seeburg PH, Takahashi R, Misawa H, Kwak S (2010) Induced loss of ADAR2 engenders slow death of motor neurons from Q/R site-unedited GluR2. J Neurosci 30: 11917-11925

Hwu WL, Muramatsu S, Tseng SH, Tzen KY, Lee NC, Chien YH, Snyder RO, Byrne BJ, Tai CH, Wu RM (2012) Gene therapy for aromatic L-amino acid decarboxylase deficiency. Sci Transl Med 4: 134ra161

Iwata N, Sekiguchi M, Hattori Y, Takahashi A, Asai M, Ji B, Higuchi M, Staufenbiel M, Muramatsu S, Saido TC (2013) Global brain delivery of neprilysin gene by intravascular administration of AAV vector in mice. Sci Rep 3: 1472

Kawahara Y, Ito K, Sun H, Aizawa H, Kanazawa I, Kwak S (2004) Glutamate receptors: RNA editing and death of motor neurons. Nature 427: 801

Kawahara Y, Ito K, Sun H, Kanazawa I, Kwak S (2003) Low editing efficiency of GluR2 mRNA is associated with a low relative abundance of ADAR2 mRNA in white matter of normal human brain. Eur J Neurosci 18: 23-33

Kwak S, Kawahara Y (2005) Deficient RNA editing of GluR2 and neuronal death in amyotropic lateral sclerosis. J Mol Med 83: 110-120

Li XG, Okada T, Kodera M, Nara Y, Takino N, Muramatsu C, Ikeguchi K, Urano F, Ichinose H, Metzger D *et al* (2006) Viral-mediated temporally controlled dopamine production in a rat model of Parkinson disease. Mol Ther 13: 160-166

Lonergan T, Teschemacher AG, Hwang DY, Kim KS, Pickering AE, Kasparov S (2005) Targeting brain stem centers of cardiovascular control using adenoviral vectors: impact of promoters on transgene expression. Physiol Genomics 20: 165-172

Mingozzi F, High KA (2011) Therapeutic in vivo gene transfer for genetic disease using AAV: progress and challenges. Nat Rev Genet 12: 341-355

Nakamura T, Takumi T, Takano A, Aoyagi N, Yoshiuchi K, Struzik ZR, Yamamoto Y (2008) Of mice and men—universality and breakdown of behavioral organization. PLoS ONE 3: e2050

Neumann M, Sampathu DM, Kwong LK, Truax AC, Micsenyi MC, Chou TT, Bruce J, Schuck T, Grossman M, Clark CM *et al* (2006) Ubiquitinated TDP-43 in frontotemporal lobar degeneration and amyotrophic lateral sclerosis. Science 314: 130-133

Nishimoto Y, Yamashita T, Hideyama T, Tsuji S, Suzuki N, Kwak S (2008) Determination of editors at the novel A-to-I editing positions. Neurosci Res 61: 201-206

Petrs-Silva H, Dinculescu A, Li Q, Deng WT, Pang JJ, Min SH, Chiodo V, Neeley AW, Govindasamy L, Bennett A *et al* (2011) Novel properties of tyrosine-mutant AAV2 vectors in the mouse retina. Mol Ther 19: 293-301

Sawada J, Yamashita T, Aizawa H, Aburakawa Y, Hasebe N, Kwak S (2009) Effects of antidepressants on GluR2 Q/R site-RNA editing in modified HeLa cell line. Neurosci Res 64: 251-258

Singh M, Kesterson RA, Jacobs MM, Joers JM, Gore JC, Emeson RB (2007) Hyperphagia-mediated obesity in transgenic mice misexpressing the RNA-editing enzyme ADAR2. J Biol Chem 282: 22448-22459

Thevenot E, Jordao JF, O'Reilly MA, Markham K, Weng YQ, Foust KD, Kaspar BK, Hynynen K, Aubert I (2012) Targeted delivery of self-complementary adeno-associated virus serotype 9 to the brain, using magnetic resonance imaging-guided focused ultrasound. Hum Gene Ther 23: 1144-1155

Yamashita T, Hideyama T, Hachiga K, Teramoto S, Takano J, Iwata N, Saido TC, Kwak S (2012a) A role for calpain-dependent cleavage of TDP-43 in amyotrophic lateral sclerosis pathology. Nat Commun 3: 1307

Yamashita T, Hideyama T, Teramoto S, Kwak S (2012b) The abnormal processing of TDP-43 is not an upstream event of reduced ADAR2 activity in ALS motor neurons. Neurosci Res 73: 153-160

Yamashita T, Tadami C, Nishimoto Y, Hideyama T, Kimura D, Suzuki T, Kwak S (2012c) RNA editing of the Q/R site of GluA2 in different cultured cell lines that constitutively express different levels of RNA editing enzyme ADAR2. Neurosci Res 73: 42-48

Neurobiology of Disease 52 (2013) 177–190

Contents lists available at SciVerse ScienceDirect

Neurobiology of Disease

journal homepage: www.elsevier.com/locate/ynbdi

# Regulation of the dopaminergic system in a murine model of aromatic L-amino acid decarboxylase deficiency

Ni-Chung Lee [a,b,c], Yih-Dar Shieh [a], Yin-Hsiu Chien [a,b], Kai-Yuan Tzen [d,e], I-Shing Yu [f], Pin-Wen Chen [a], Min-Hsiu Hu [a], Meng-kai Hu [a], Shin-ichi Muramatsu [g], Hiroshi Ichinose [h], Wuh-Liang Hwu [a,b,*]

[a] Department of Medical Genetics, National Taiwan University Hospital and National Taiwan University College of Medicine: 8 Chung-Shan South Road, Taipei 10041, Taiwan
[b] Department of Pediatrics, National Taiwan University Hospital and National Taiwan University College of Medicine: 8 Chung-Shan South Road, Taipei 10041, Taiwan
[c] Graduate Institute of Clinical Medicine, National Taiwan University College of Medicine: 7, Chung-Shan South Road, Taipei 10002, Taiwan
[d] Department of Nuclear Medicine, National Taiwan University Hospital and National Taiwan University College of Medicine: 7, Chung-Shan South Road, Taipei 10002, Taiwan
[e] Molecular Imaging Center, National Taiwan University, Taipei, Taiwan
[f] Laboratory Medicine, National Taiwan University Hospital and National Taiwan University College of Medicine: 8 Chung-Shan South Road, Taipei 10041, Taiwan
[g] Division of Neurology, Department of Medicine, Jichi Medical University: 3311-1 Yakushiji, Shimotsuke, Tochigi 329-0498, Japan
[h] Department of Life Science, Graduate School of Bioscience and Biotechnology, Tokyo Institute of Technology, Yokohama 226-8501, Japan

ARTICLE INFO

*Article history:*
Received 8 September 2012
Revised 10 December 2012
Accepted 14 December 2012
Available online 26 December 2012

*Keywords:*
Aromatic L-amino acid decarboxylase deficiency
Mouse knock-in model
Neurotransmitter
Dopamine
Serotonin
Dyskinesia
Splicing

ABSTRACT

Aromatic L-amino acid decarboxylase (AADC) is responsible for the syntheses of dopamine and serotonin. Children with AADC deficiency exhibit compromised development, particularly with regard to their motor functions. Currently, no animal model of AADC deficiency exists. We inserted an AADC gene mutation (IVS6+4A>T) and a neomycin-resistance gene into intron 6 of the mouse AADC (*Ddc*) gene. In the brains of homozygous knock-in (KI) mice ($Ddc^{IVS6/IVS6}$), AADC mRNA lacked exon 6, and AADC activity was <0.3% of that in wild-type mice. Half of the KI mice were born alive but grew poorly and exhibited severe dyskinesia and hindlimb clasping after birth. Two-thirds of the live-born KI mice survived the weaning period, with subsequent improvements in their growth and motor functions; however, these mice still displayed cardiovascular dysfunction and behavioral problems due to serotonin deficiencies. The brain dopamine levels in the KI mice increased from 9.39% of the levels in wild-type mice at 2 weeks of age to 37.86% of the levels in wild-type mice at 8 weeks of age. Adult KI mice also exhibited an exaggerated response to apomorphine and an elevation of striatal c-Fos expression, suggesting post-synaptic adaptations. Therefore, we generated an AADC deficient mouse model, in which compensatory regulation allowed the mice to survive to adulthood. This mouse model will be useful both for developing gene therapies for AADC deficiency and for designing treatments for diseases associated with neurotransmitter deficiency.


## Introduction

Aromatic L-amino acid decarboxylase (AADC, EC 4.1.1.28) is a homodimeric pyridoxal phosphate-dependent enzyme involved in the metabolic pathways responsible for the syntheses of two monoamine neurotransmitters, dopamine and serotonin (Hamosh and McKusick, 2011). AADC decarboxylates L-3,4-dihydroxyphenylalanine (L-DOPA) to dopamine, L-5-hydroxytryptophan to serotonin, and L-tryptophan to tryptamine (Consortium, 2011; Hamosh and McKusick, 2011). Dopamine is the precursor of catecholaminergic hormones and is also itself a neurotransmitter in the basal ganglia. Dopamine is responsible for reward-driven learning, voluntary movement control, feeding, neuroendocrine secretion, cognition, and behavior (Crittenden and Graybiel, 2011; Hamosh and McKusick, 2011). Serotonin has important neuromodulatory actions in cognitive, emotional, impulse control, circadian rhythm, sleep–wake cycle, pain, respiratory, and cardiovascular functions (Benarroch, 2009). AADC also mediates the syntheses of trace amines (Berry, 2004).

Defects in the AADC gene result in a deficiency of dopamine and serotonin and their downstream metabolites. AADC deficiency (MIM #608643) is an autosomal recessive inborn error of metabolism and was first identified in 1990 by Hyland and Clayton (Hyland and Clayton, 1990; Hyland et al., 1992). Approximately eighty cases were reported worldwide between 1990 and 2010 (Abeling et al., 1998; Brautigam et al., 2000; Brun et al., 2010; Fiumara et al., 2002; Korenke et al., 1997; Maller et al., 1997; Pons et al., 2004; Swoboda et al., 1999; Swoboda et al., 2003; Tay et al., 2007). Clinical manifestations of AADC deficiency include hypotonia, hypokinesia, oculogyric crises, and signs of autonomic dysfunction, beginning early in life (Brun et al., 2010).

* Corresponding author at: Department of Medical Genetics, Room 19005, 19F, Children's Hospital Building, National Taiwan University Hospital, 8 Chung-Shan South Road, Taipei 10041, Taiwan. Fax: +886 2 23314518.
*E-mail addresses:* ncleentu@ntu.edu.tw (N.-C. Lee), sam8913105@yahoo.com.tw (Y.-D. Shieh), chienyh@ntu.edu.tw (Y.-H. Chien), tzenky@ntuh.gov.tw (K.-Y. Tzen), oxfo32@yahoo.com.tw (I.-S. Yu), musyhkai@yahoo.com.tw (P.-W. Chen), muramats@jichi.ac.jp (S. Muramatsu), hichinos@bio.titech.ac.jp (H. Ichinose), hwuwlntu@ntu.edu.tw (W.-L. Hwu).
**Available online on ScienceDirect (www.sciencedirect.com).**

0969-9961/$ – see front matter © 2013 Elsevier Inc. All rights reserved.
http://dx.doi.org/10.1016/j.nbd.2012.12.005

AADC deficiency is comparatively less rare in Taiwan relative to other countries because of a splice site mutation (IVS6+4A>T) in the Taiwanese population (Brun et al., 2010). This mutation interrupts the donor consensus sequence of intron 6, which causes aberrant splicing of the gene (Lee et al., 2009; Tay et al., 2007).

L-DOPA is an effective drug for Parkinson's disease and tyrosine hydroxylase (TH) deficiency. However, L-DOPA cannot be converted to dopamine in cases of AADC deficiency, and dopamine does not cross the blood–brain barrier. Patients with AADC deficiency only partially respond to dopamine agonists, and many patients die during childhood (Pons et al., 2004). Recently, gene therapy was tested in patients with AADC deficiencies (Hwu et al., 2012). The treatment employed an adeno-associated virus vector that was injected into the bilateral putamen of patients to replenish AADC levels. Gene therapy improves the motor function of patients and decreases the severity of oculogyric crisis. However, the development of a treatment for AADC deficiency is still hampered by the lack of an animal model of the disease.

Knockout of the mouse AADC (*Ddc*) gene results in death in utero (unpublished observation by H.I.). Therefore, in this study, we employed a knock-in (KI) strategy by inserting an IVS6+4A>T mutation into the mouse AADC gene. Homozygous KI mice were able to survive into adulthood and exhibited biochemical and movement abnormalities similar to those observed in patients with AADC deficiencies.

## Materials and methods

### *Generating the KI mice*

An artificial mouse bacterial chromosome containing exon 6 and intron 6 of the AADC gene was obtained from a 129/SvJ genomic library. The KI vector was constructed by the Transgenic Mouse Model Core Facility (Liu et al., 2003), and Southern blot analyses were performed to select KI embryonic stem (ES) cells, as previously described (Su et al., 2007). The AADC genotype was determined by polymerase chain reaction (PCR) using the primers 5′-AGGCGCATTCCTCTGTAGAA and 5′-CCCAAATAGTGCCAACACCT, followed by direct sequencing. Heterozygous ES cell clones ($Ddc^{+/IVS6}$) were microinjected into 129/B6 blastocysts and then transferred into pseudopregnant females to generate chimeras. The chimeric mice were mated with B6 mice to generate heterozygous F1 mice. Mice were housed under standard conditions with artificial 12-h dark–light cycles. Behavioral tests, tissue sampling, blood sampling, and imaging analyses were performed on homozygous ($Ddc^{IVS6/IVS6}$) KI mice at 2, 4, 8, and 12 weeks of age. Either wild-type or heterozygous littermates were used as controls. These animal studies were approved and performed in accordance with the guidelines of the National Taiwan University College of Medicine and College of Public Health Institutional Animal Care and Use Committee (IACUC no. 2110134).

### *RNA analyses*

Mice were sedated with avertin (0.3–0.4 μg/g body weight) before euthanasia. Coronal slices of the brain containing either the striatum or the substantia nigra were homogenized with Trizol® for RNA studies. Total RNA was extracted using the Trizol® reagent according to the manufacturer's protocol. The reverse transcription (RT) reaction mixture included 2 μg of RNA and 0.5 μg of oligo(dT). The PCR reactions either included exon 6 using the primers 5′-ACTGGCTGCTCGGACTAAAG and 5′-CCCACTTCCAGGAGATTGTC or were specific to exon 6 using the primers 5′-CATGAGAGCTTCTGCCCTTC (located on exon 6) and 5′-GCAAACTCCACACCATTCAG; the latter was used for mRNA quantitation. The genes amplified and the PCR primers used are as follows: mouse dopamine active transporter (DAT; *Slc6a3*), 5′-TGCTGGTCATTGTTCTGCTC and 5′-TATGCTCTGATGCCATCCAT; vesicular monoamine transporter 2 (VMAT2; *Slc18a2*), 5′-CAAGCTGATCCTGTTCATCG and 5′-GGAAGTGGA GGCTGTGAGC; TH (*Th*), 5′-CGTCATGCCTCCTCACCTAT and 5′-CCCAGAG ATGCAAGTCCAAT; catechol-*O*-methyltransferase (COMT; *comt*), 5′-CTGACTACGCTGCCATCACC and 5′-TAGCGGTCTTTCCAGTGGTC; c-Fos (*c-fos*), 5′-GAATGGTGAAGACCGTGTCA and 5′-GCAGCCATCTTATTCCGT TC; substance P (protachykinin-1; *Tac1*), 5′-GGATGCTGATTCCTCAGTTG and 5′-TAGTTCTGCATCGCGCTTCT; dynorphin (prodynorphin; *Pdyn*), 5′-TGCAGTGAGGATTCAGGATG and 5′-GCAACCTCATCTTCCAAGTCA; enkephalin (preproenkephalin; *Penk*), 5′-CCTGCCTCCTGGCTACAGT and 5′-GCAGGAGATCCTTGCAGGT; and *β-actin*, 5′-GCTACAGCTTCACCACCACA and 5′-TCTCCAGGGAGGAAGAGGAT. Quantitative PCR results were expressed as $2^{-\Delta\Delta CT}$, representing the quantity of PCR products of KI mice relative to that of wild-type mice after normalization to the quantity of *β-actin* (Livak and Schmittgen, 2001).

### *Western blot, immunohistochemistry (IHC), and immunofluorescence (IF) analyses*

Mouse brain coronal slices were snap frozen in liquid nitrogen and stored at −80 °C for western blot analyses using TH (1:1000, Millipore, Billerica, MA, USA), AADC (1:1500, Abcam, Cambridge, UK), or tubulin (1:1500, MDBio, Taipei, Taiwan) antibodies. Mouse striatum was isolated for western blot analyses using dopamine D1 receptor (1:500, Santa Cruz Biotechnology Inc., Santa Cruz, CA, USA), D2 receptor (1:500, Santa Cruz Biotechnology Inc., Santa Cruz, CA, USA), and MAOA (1:500, Proteintech) antibodies. For IHC and IF studies, mice were perfused with 4% paraformaldehyde. The brains were removed, post-fixed overnight at 4 °C, cryoprotected with 30% sucrose in phosphate-buffered saline (PBS) for 48 h, mounted in OCT embedding compound, and frozen. Coronal sections (40 μm in thickness) were cut on a cryostat and collected in PBS. IHC was performed by incubation overnight with TH (1:50,000) (Nagatsu et al., 1979) or AADC (1:20,000) antibodies (Nagatsu et al., 1988). The slides were washed, incubated for 2 h with a biotinylated anti-rabbit IgG secondary antibody (1:200, Vector Laboratories, Burlingame, CA, USA), and visualized using the VECTASTAIN Elite ABC Kit and Peroxidase Substrate DAB Kit (both from Vector Laboratories, Burlingame, CA, USA). Dual IF staining for TH and AADC was performed by incubation with a mixture of TH (1:800, ImmunoStar, Hudson, WI, USA) and AADC (1:5000) antibodies, followed by Alexa Fluor 594-labeled anti-rabbit IgG and Alexa Fluor 488-labeled anti-mouse IgG secondary antibodies (both from Life Technologies, Grand Island, NY, USA). The sections were viewed and photographed with a confocal laser scanning microscope (FV10i, Olympus, Tokyo, Japan). Total numbers of AADC- and TH-stained neurons throughout the entire substantia nigra were counted stereologically in a blinded fashion with Stereo Investigator software (MBF Bioscience, Williston, VT, USA) using the Optical Fractionator Probe module. Coronal sections (10 μm in thickness) were also cut for IHC with c-Fos (1:300, Santa Cruz Biotechnology Inc., Santa Cruz, CA, USA) and serotonin reuptake transporter (SERT, 1:500, Millipore, Billerica, MA, USA) antibodies. For c-Fos staining, adult mice (8 weeks of age) were injected with apomorphine subcutaneously 2 h before sacrifice. The number of c-Fos-positive nuclei in the striatum was quantified under a light microscope. Three serial sections were stained, counted, and averaged for each striatum.

### *Positron emission tomography (PET)*

PET was performed as previously reported (Lin et al., 2010; Vuckovic et al., 2010). For 6-[$^{18}$F]fluoro-L-DOPA (FDOPA) PET, mice were treated with carbidopa (25 mg/kg, i.p.) and entacapone (25 mg/kg, i.p.) 30 min before the injection of FDOPA (250 μCi for 2-week-old mice and 500 μCi for 8-week-old mice, i.p.). Thirty min after FDOPA injection, mice were anesthetized with isoflurane, and images were obtained using a small animal PET/CT scanner (eXplore Vista DR, GE Healthcare, Fairfield, CT, USA).

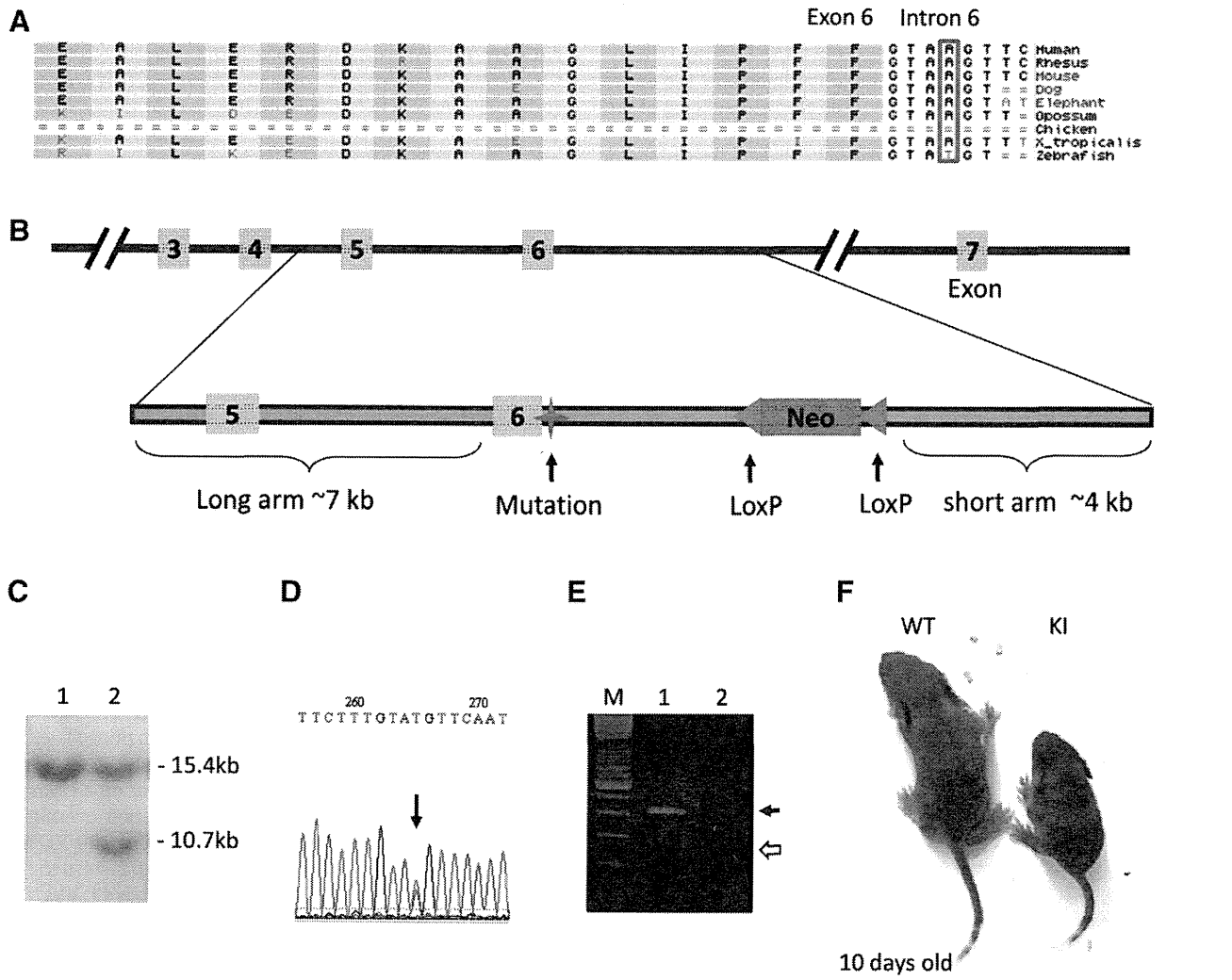


**Fig. 1.** Knock-in (KI) embryonic stem (ES) cells demonstrate splicing errors. (A) A BLAST analysis using the UCSC Genome Browser revealed sequence conservation at the intron 6 donor site of the AADC gene. (B) The KI construct contains a mutation generated by mutagenesis at the intron 6 donor site and a *neo* gene cassette inserted into intron 6. (C) Southern blot analyses after *Bam*HI digestion revealed an additional 10.7-kb product in the heterozygous KI ($Ddc^{+/IVS6}$) ES cells (lane 2) but not in the parental ES cells (lane 1). (D) Direct sequencing of the KI ES cell DNA revealed a heterozygous A to T mutation (arrow). (E) RT-PCR of exon 6 for two KI ES clones (lanes 1 and 2) revealed two products: the full-length (arrow) and the exon 6-deleted (open arrow) mRNAs, where M denotes the molecular weight marker. (F) A photograph of the mice. The homozygous KI mouse (right side) is much smaller than the wild-type (WT) mouse (left side) at 10 days of age.

*AADC activity and neurotransmitter levels*

Whole brains from mice were snap-frozen in liquid nitrogen and stored at −80 °C for AADC activity and neurotransmitter analyses. AADC activity in brain homogenates was assayed based on the measurement of enzymatically formed dopamine, with L-DOPA as a substrate, using high-performance liquid chromatography (HPLC) with electrochemical detection after separation with an Amberlite CG-50 column (Ichinose et al., 1985). The standard incubation mixture (a total volume of 400 μl) contained 30 mM sodium phosphate buffer (pH 7.2), 0.17 mM ascorbic acid, 0.1 mM pargyline HCl (a monoamine oxidase inhibitor), 0.01 mM pyridoxal phosphate, 1.0 mM L-DOPA (or D-DOPA for the blank), and the enzyme reaction was carried out at 37 °C for 20 min. For measuring neurotransmitter levels, tissues were deproteinized by 0.2 M perchloric acid and centrifuged at 15,000 ×g for 10 min. L-DOPA, dopamine, 3, 4-dihydroxyphenylacetic acid (DOPAC), homovanillic acid (HVA), norepinephrine (NE), 5-hydroxytryptamine (5-HT, serotonin), and 5-hydroxyindoleacetic acid (5-HIAA) levels were analyzed by HPLC using a previously reported protocol (Homma et al., 2011). To investigate if brain dopamine was synthesized from tyramine, mice were first treated with reserpine (10 mg/kg i.p., Sigma Aldrich, St. Louis, MO, USA) 18.5 h before being sacrificed to deplete the vesicular stores of dopamine (Bromek et al., 2011). On the day of the experiment, mice were further treated with either α-methyl-*p*-tyrosine (α-MT, 300 mg/kg i.p., Sigma Aldrich, St. Louis, MO, USA) 3.5 h before sacrificing to inhibit TH, or quinine (50 mg/kg i.p., Alfa Aesar, Ward Hill, USA) 1.25 h before sacrificing to inhibit the alternative pathway enzyme CYP2D. Brain DOPAC levels were then measured.

*Motor and behavioral tests*

Hindlimb clasping was measured by hanging mice by their tails. The score was 1 for any dystonic movement and 0 for no abnormal movement. The total clasping score was calculated by adding up the scores in 2-s segments for 24 s (Gantois et al., 2007). Four-limb akinesia was measured by hanging the mice by their tails and then slowly placing them on the ground (Yang et al., 2006). The time required to move all four limbs and walk was then recorded. Rotarod tests were performed using machines with 3-cm-diameter spindles (Ugo Basile, Varese, Italy) (Rozas et al., 1997). Infant mice were trained at 16 rpm for 60 s; this training was repeated four times. After resting for 15 min, the mice were tested using five speeds (16, 20, 24, 28, and 32 rpm). Each session lasted up to 120 s, and the time required for falling from the rod (the latency) was recorded.

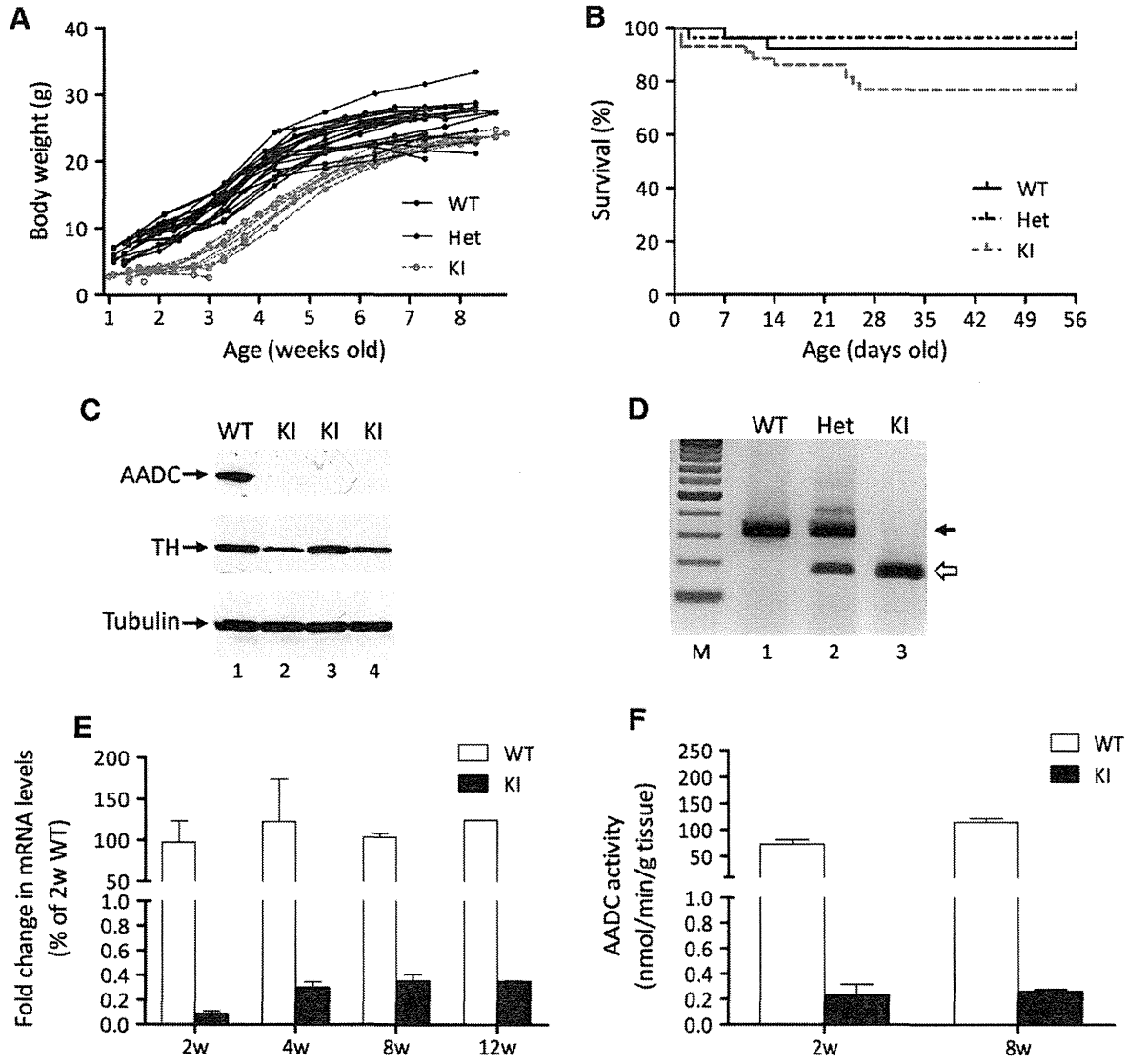


**Fig. 2.** Poor weight gain and decreased survival rate due to a deficiency in AADC expression. (A) Body weight curves of homozygous KI (KI, blue, n = 10), heterozygous KI (Het, black, n = 11), and wild-type (WT, red, n = 10) mice. The homozygous KI mice exhibited low body weights from birth but normal growth rates after 3 weeks of age. Each line represents an individual mouse. (B) Survival curves. The survival rate was 92.3% for wild-type mice and 67.7% for KI mice ($p = 0.01$; WT n = 31, Het n = 65, KI n = 45). (C) Western blot analyses of TH and AADC proteins in the brains of 2-week-old mice. In the KI mice, the AADC protein was not detectable (lanes 2–4); the TH protein was detectable, but the expression levels were variable. A total of 20 μg of brain homogenate was loaded in each lane. Tubulin was used as a control. (D) Brain AADC mRNA RT-PCR of exon 6. The full-length product (arrow) was detected in wild-type and heterozygous mice, but only the exon 6-deleted product (open arrow) was detected in the KI mice (lane 3). (E) Quantitative RT-PCR using primers specific to full-length mRNA revealed that the mRNA levels in the KI mice were <0.5% of the levels in age-matched wild-type mice. The data were normalized to the quantity of β-actin mRNA. (F) AADC activity measured in the brain homogenates. The activity in the KI mice was only 0.2–0.3% than that in the wild-type mice.

Adult mice were trained at 0 rpm for 60 s (repeated 3 times) and 4 rpm for 60 s (repeated three times). The mice were subsequently tested at an accelerating speed from 4 to 40 rpm over 300 s. The latency and the speed of the rod at the time of falling were recorded.

Blood pressures and heart rates were measured under general anesthesia using the BP-2000 Series II Blood Pressure Analysis System (Visitech Systems, Inc., Apex, NC, USA); measurements were repeated 10 times/afternoon on three consecutive afternoons. Electrocardiography (ECG) was recorded under general anesthesia using PowerLab 8/30 to measure the RR interval, PR interval, P duration, QRS duration, QT interval, and QTc.

Home cage activities, such as travel distance, awakening, drinking, feeding, grooming, hanging, rearing up, resting, twitching, and walking, were recorded over a 24-h period and analyzed using Clever Sys HomeCageScan TM3.0 (Clever Sys., Inc., Reston, VA, USA). Open field activities were recorded and calculated using Clever Sys TopScanT (Clever Sys., Inc., Reston, VA, USA). Mice were placed separately in an arena and observed for 1 h for total distance moved, rearing, and location (time spent in the central part of the arena, ratio of the locomotion in the center of the arena to the total locomotion, and latency to enter the central part of the arena). The elevated plus maze was arranged to evaluate anxiety-related behavior according to a previous report (Wu et al., 2010). The test was performed in a Plexiglas plus maze (size: 65 × 65 cm) equipped with the video-based EthoVision Color-Pro system (Noldus Information Technology, Wageningen, Netherland). Mice were also injected with apomorphine (1.0 mg/kg, i.p.), and their total activity and number of rears were recorded for 10 min by an automated locomotor activity analyses system (PAS-Open Field, San Diego Instruments, San Diego, CA, USA).

### *Statistics*

Data are presented as the means ± SEMs in each figure. Statistical analyses were performed using the SPSS statistical package, version

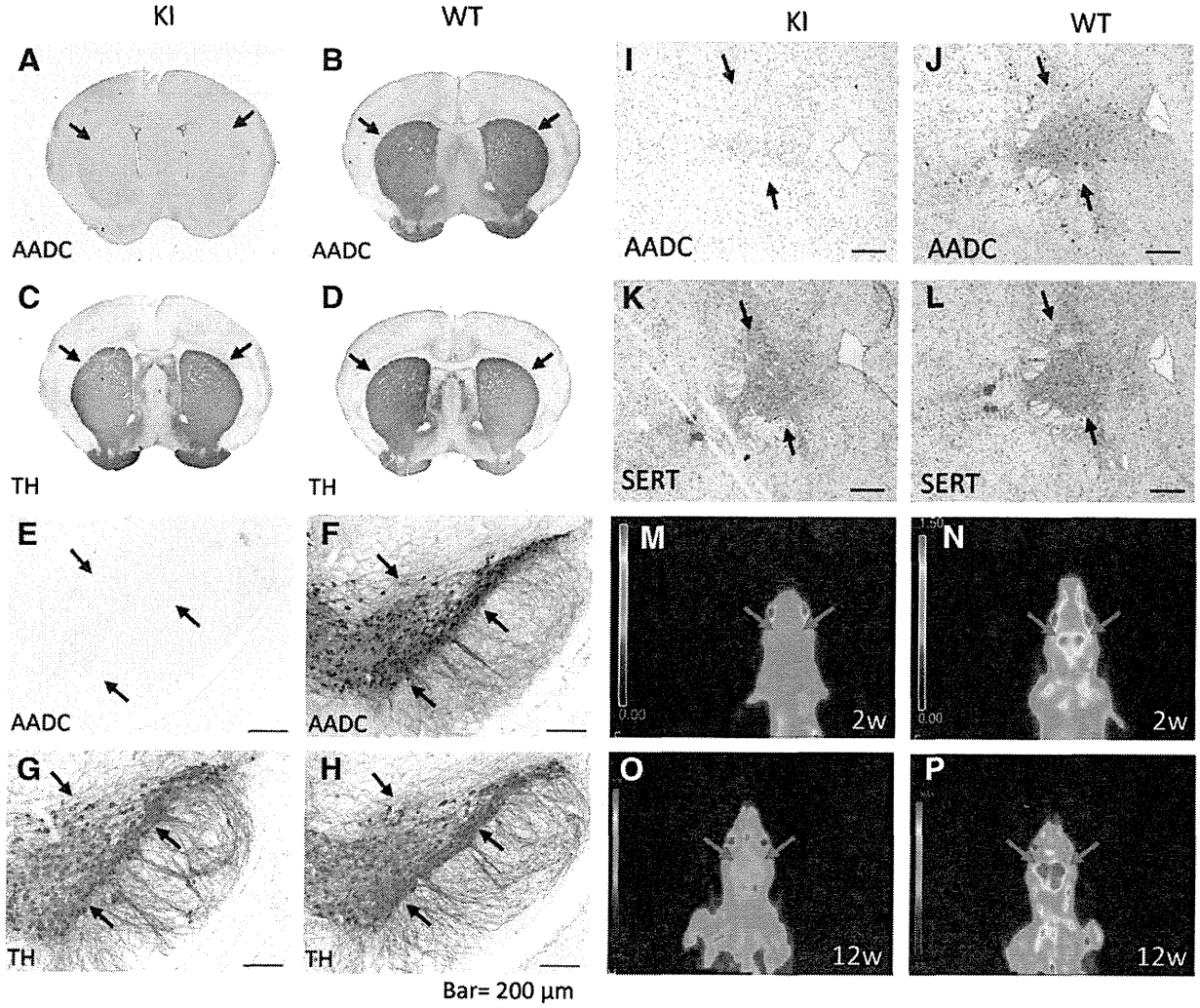


**Fig. 3.** Immunohistochemical staining showed no AADC expression in the adult (8 weeks of age) KI mouse brain. (A) Absence of AADC staining in the KI mice striatum (arrows). (B) Normal AADC staining in the wild-type mice striatum. (C) Normal TH staining in the KI mice striatum. (D) Normal TH staining in the wild-type mice striatum. (E) Absence of AADC staining in the KI mice substantia nigra (between the arrows), 400×. (F) Normal AADC staining in the wild-type mice substantia nigra. (G) Normal TH staining in the KI mice substantia nigra. (H) Normal TH staining in the wild-type mice substantia nigra. (I) Absence of AADC staining in the dorsal raphe nucleus of the KI mice (between the arrows), 50×. (J) Normal AADC staining in the dorsal raphe nucleus of the wild-type mice. (K) Normal SERT staining in the dorsal raphe nucleus of the KI mice. (L) Normal SERT staining in the dorsal raphe nucleus of the wild-type mice. (M through O) 6-[$^{18}$F]fluoro-L-dopa (FDOPA) positron emission tomography (PET) scans showed no signal in the KI mice. (M) No PET signal in the striatum of infant (2 weeks of age) KI mice (arrows). (N) Normal PET signal in the striatum of infant wild-type mice. (O) No PET signal in the striatum of adult (12 weeks of age) KI mice. (P) Normal PET signal in the striatum of adult wild-type mice.

11.5. The Student's t test or Mann–Whitney rank test was applied for statistical analyses between different groups. The log-rank test was used to analyze the survival rate. A $p$ value$<0.05$ was considered statistically significant.

## Results

### *Producing the IVS6+4A>T KI Mice*

Mouse (NM_001190448.1) (Bruneau et al., 1992) and human (NM_000790) AADC genes (Sumi-Ichinose et al., 1992) are highly conserved at the intron 6 donor site (Fig. 1A). The KI vector contains a mutation at the intron 6 donor site and a *neo* gene cassette flanked by a *loxP* site in intron 6 (Fig. 1B). The KI ES cells were screened using Southern blot analyses to identify the *Bam*HI restriction site introduced by the *neo* cassette (Fig. 1C). The presence of a heterozygous IVS6+4A>T mutation was further confirmed by direct sequencing (Fig. 1D). This splicing site mutation, in the presence of the *neo* gene cassette in intron 6, resulted in aberrant RNA splicing, which skips exon 6 in the ES cells (Fig. 1E). Removal of the *neo* cassette resulted in an increase in normally spliced AADC mRNA, which essentially erased all symptoms in the KI mice (data not shown). The heterozygous KI mice ($Ddc^{+/IVS6}$) displayed no abnormal phenotype. Only half of the homozygous KI mice ($Ddc^{IVS6/IVS6}$) were born alive, and these mice were undistinguishable from normal littermates on the day of birth. After birth, the KI mice grew poorly, and at 10 days of age, they were much smaller than the wild-type mice (Fig. 1F).

### *Poor growth and abnormal AADC gene expression*

The KI mice grew poorly after birth. Suckling was observed; however, the KI mice often exhibited sunken abdomens. However, if the KI mice survived until weaning, their growth rate became normal (Fig. 2A). The survival rate of the live-born KI mice was 67.7% (Fig. 2B). AADC protein expression was not detected in the substantia nigra of the KI mice, as determined by western blot analyses (Fig. 2C). Western blot analyses of TH displayed some variability, which may be a result of slicing the substantia nigra region from the brain (Fig. 2C, lanes 2 and 4). A majority of the AADC mRNA in the KI mouse brain lacked exon 6, a similar result to that observed in the ES cells (Fig. 2D). Quantitative RT-PCR analyses revealed that the amount of

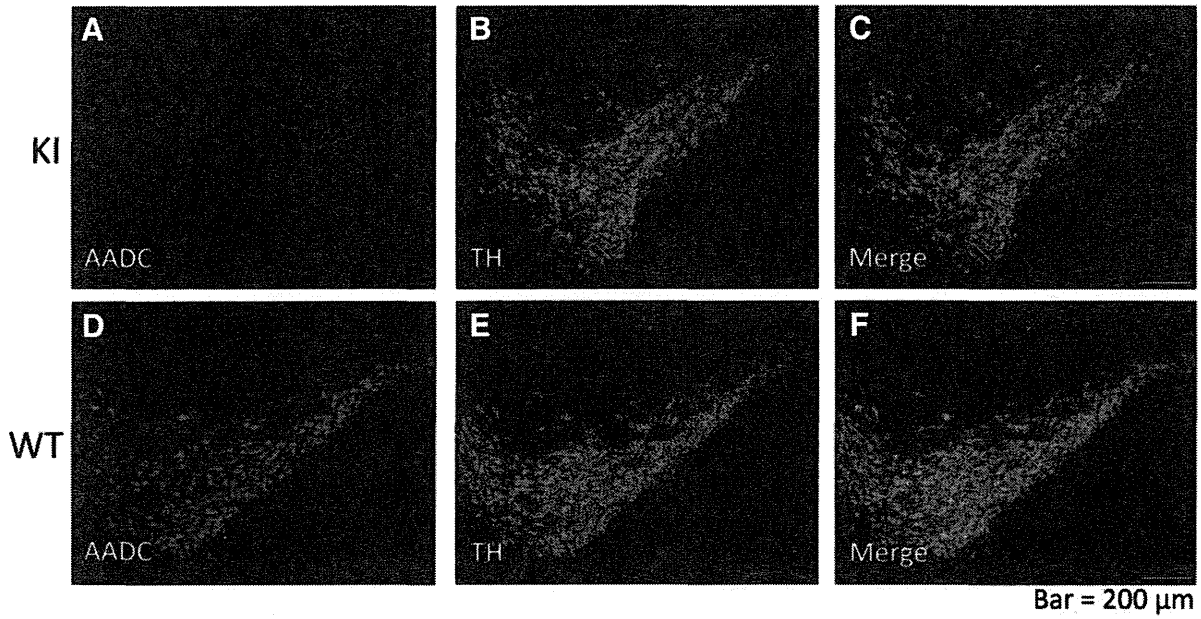


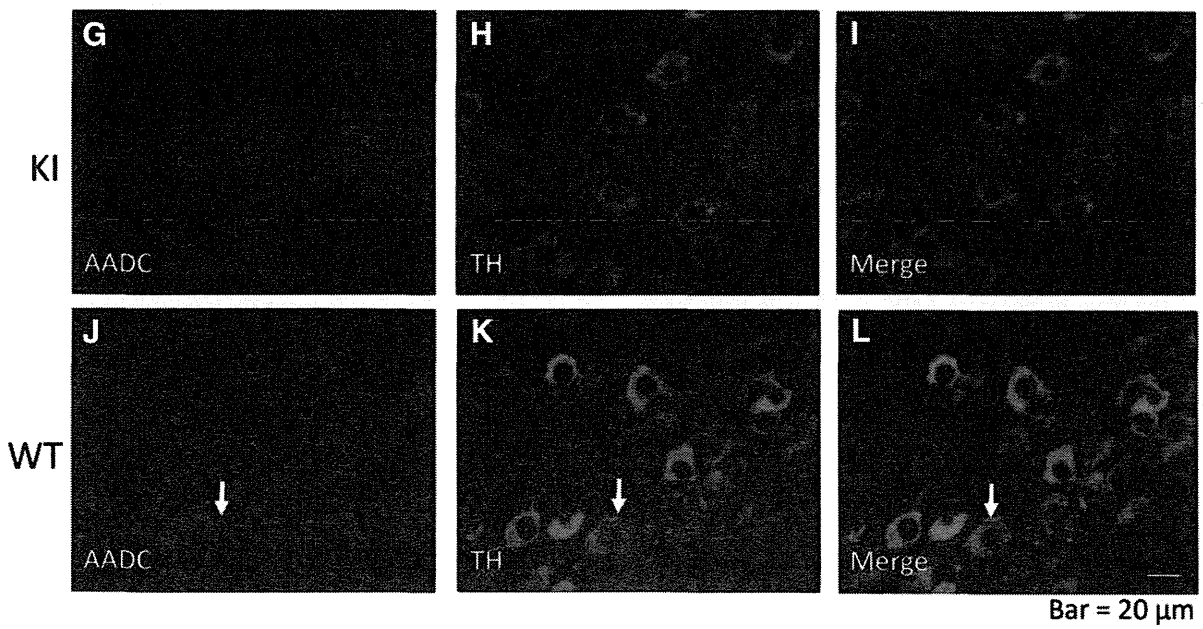


M

| Stain | Genotype | Positive Cell Number | | |
|---|---|---|---|---|
| | | Mean | SD | SE |
| AADC | WT | 12537.6 | 1247.3 | 720.1 |
| | KI | 0.0 | 0.0 | 0 |
| TH | WT | 11639.0 | 1032.2 | 596.0 |
| | KI | 10019.6 | 1068.6 | 617.0 |

SD, standard deviation; SE, standard error; n=3

N

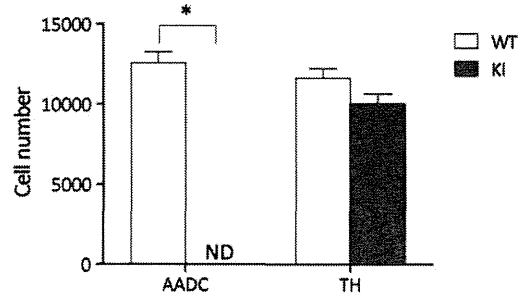


**Fig. 4.** AADC and TH dual immunofluorescence in the substantia nigra of 8-week-old mice. (A through F) Low magnification (100×) views of the substantia nigra showed that the KI mice exhibited negative AADC (red) staining (A) but normal TH (green) staining, while the wild-type mice showed both AADC (D) and TH (E) staining, and the staining overlapped completely (F). (G through L) High magnification (600×) views of the substantia nigra displaying individual cells. The arrow in panel J, K, and L points to one typical cell where the red (J) and green (K) colors were merged into an orange color (L). (M) Total numbers of AADC- and TH-stained neurons throughout the entire substantia nigra were counted stereologically. (N) Quantitative results of M.

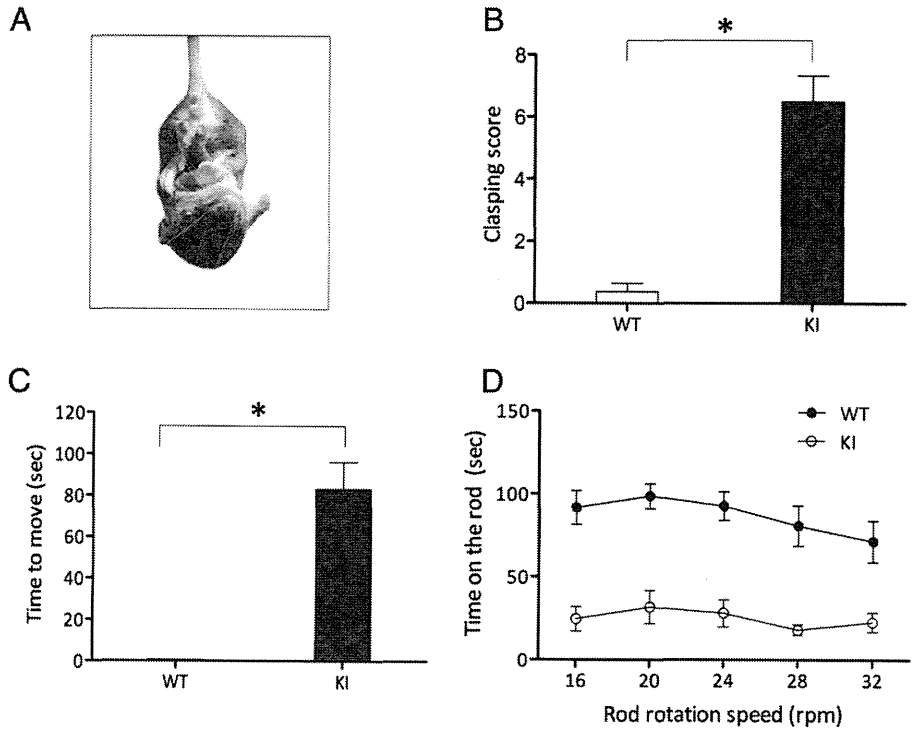


**Fig. 5.** Infant (2-week-old) KI mice displayed severe motor dysfunction. (A) A picture of hindlimb clasping. (B) The hindlimb clasping score was much higher in the KI mice than in the wild-type mice ($p<0.001$). (C) Four-limb akinesia test. The KI mice had a significant delay in moving their four limbs after being placed on the ground following tail hanging ($p<0.001$). (D) Latency to fall in the rotarod test. The KI mice exhibited a shorter latency to fall off the rotarod than the wild-type mice ($p<0.05$ for all speeds, n = 12). * indicates $p<0.05$.

full-length mRNA in the KI mice was <0.5% of that in age-matched wild-type mice (Fig. 2E). We measured the brain AADC activity in infant (2 weeks old) and adult (8 weeks old) KI mice. The results revealed that the brain homogenate AADC activities in both infant (2 weeks old) and adult (8 weeks old) KI mice were 0.2–0.3% of that in the AADC activities in age-matched wild-type mice (Fig. 2F).

*Absence of AADC expression in the brain*

In the IHC studies, the striata of KI mice were negative for AADC staining (Fig. 3A), although the TH staining was normal (Fig. 3C). The staining from wild-type mice is shown for comparison (Figs. 3, B and D). The substantia nigra of the KI mice did not demonstrate AADC staining (Fig. 3E) but showed normal TH staining (Fig. 3G) when compared with the staining in the substantia nigra of wild-type mice (Figs. 3, F and H). Similarly, the dorsal raphe nucleus of the KI mice did not show AADC staining (Fig. 3I) but showed normal SERT staining (Fig. 3K) when compared with the staining in wild-type mice (Figs. 3, J and L). In the FDOPA PET scans, which indicate AADC activity, the striata could be visualized in infant and adult (12 weeks of age) wild-type mice (Figs. 3, N and P, respectively) but not in KI mice (Figs. 3, M and O). Upon dual IF staining for AADC and TH, most of the TH-positive cells were also positive for AADC in the wild-type mice (Figs. 4, F and L). However, in KI mice, the TH-positive cells were negative for AADC staining (Figs. 4, C and I). We counted stereologically the total numbers of TH-stained neurons throughout the entire substantia nigra in both KI and wild-type mice, and there were no differences between them (Figs. 4, M and N).

*Motor and cardiovascular dysfunctions*

Infant KI mice displayed delayed eye-opening and ptosis, were hypoactive and dyskinetic, and exhibited resting tremors (Video 1). When the KI mice were hung by their tails, they exhibited hindlimb clasping (Fig. 5A), which was rarely observed for wild-type mice (Fig. 5B; $p<0.001$). In the four-limb akinesia test, in which mice were placed on the ground after they had been hung by their tails, the KI mice were slower to move their four limbs and walk than the wild-type mice were (Fig. 5C; $p<0.001$). In the rotarod test, the KI mice fell earlier from the rod than the wild-type or heterozygous mice (Fig. 5D; $p<0.05$). When the KI mice gained weight after weaning, their motor functions gradually improved. Adult KI mice of 6–10 weeks of age were normal in terms of size and movements and were visually indistinguishable from the wild-type mice (Video 2). However, in a rotarod test with an accelerating speed and minimal training, the adult mice tended to fall earlier (Fig. 6A; $p=0.056$) and at lower speeds (Fig. 6B; $p=0.056$) when compared with wild-type mice. Repeated rotarod tests of the same mice later yielded normal results. Therefore, adult KI mice are likely to display impairments in learning new motor skills. Additionally, adult KI mice had lower systolic blood pressures (Fig. 6C; $p=0.009$) and lower heart rates (Fig. 6E; $p=0.028$) than those of wild-type mice. These cardiovascular dysfunctions are part of the autonomic dysfunction observed in patients with AADC deficiency (Swoboda et al., 2003), and are likely related to the lack of epinephrine and norepinephrine. A mouse model deficient of dopamine β-hydroxylase (DBH), which is responsible for the production of epinephrine and norepinephrine from dopamine, has been created. The $Dbh^{-/-}$ mice had a low heart rate and were severely hypotensive (Swoap et al., 2004).

*Behavioral problems*

The adult KI mice were fertile but exhibited poor maternal care. In the home cage test for evaluating unconstrained behaviors, the KI mice demonstrated more twitching both in the daytime ($p=0.032$) and nighttime ($p=0.008$) (Fig. 7A) and spent less time hanging in the daytime (Fig. 7B; $p=0.008$). When the KI mice were placed in an open field, they tended to spend less time in the center of the

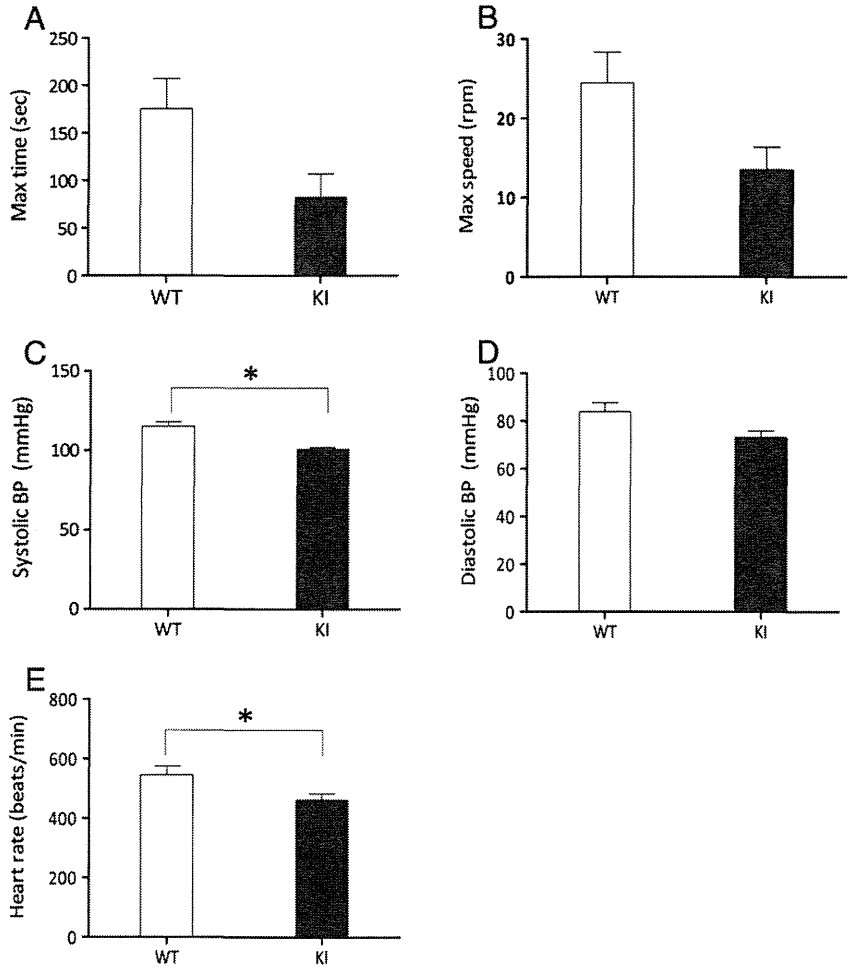


**Fig. 6.** Motor and cardiovascular dysfunctions in adult KI mice. (A and B) Mice that were 8–10 weeks of age were tested on an accelerating speed rotarod (n = 5, triplicate tests). (A) Latency to fall. The KI mice fell slightly faster than the wild-type mice ($p = 0.056$). (B) Rotarod speed at falling. The KI mice fell at slightly lower speeds than the wild-type mice ($p = 0.056$). (C through E) Blood pressure and heart rate measurements in 6–7-week-old mice (n = 5). (C) The KI mice had a lower systolic blood pressure ($p = 0.009$). (D) The KI mice might have a lower diastolic blood pressure ($p = 0.075$). (E) The KI mice had a lower heart rate ($p = 0.028$). * indicates $p < 0.05$.

cage (Fig. 7C; $p = 0.076$) and had a longer latency before they entered the center of the cage (Fig. 7D; $p = 0.175$) than that of wild-type mice. To verify if the KI mice displayed higher anxiety or fear, we utilized the elevated plus maze test, which is based on rodents' aversion of open spaces. In this test, the KI mice had lower general activity according to the total distance moved (Fig. 8A; $p = 0.002$) and the total number of arm entries (Fig. 8B; $p = 0.000$). The KI mice spent a significantly greater proportion of time in the closed arms ($p = 0.001$) and less time in the open arms (Fig. 8C; $p = 0.049$) or at the center ($p = 0.001$). The elevated plus maze test confirmed that the KI mice displayed higher anxiety levels.

*Neurotransmitter deficiencies*

In whole mouse brain homogenates, L-DOPA, a precursor of dopamine, accumulated in the KI mice but not in the wild-type mice only in the KI mice, particularly when they were young (Fig. 9A). The dopamine (Fig. 9B), norepinephrine (Fig. 9E), and serotonin (Fig. 9F) levels were lower in the KI mice than in the wild-type mice. Metabolites of these neurotransmitters, including DOPAC (Fig. 9C), HVA (Fig. 9D), and 5-HIAA (Fig. 9G), were also low in the KI mice. Moreover, the adult KI mice (8 weeks of age) had a relatively higher neurotransmitter level than the infant KI mice. For example, in KI mice, the dopamine levels increased from 9.39% of those in infant wild-type mice ($p = 0.021$) to 37.86% of those in adult wild-type mice (8 weeks of age) ($p = 0.050$) (Fig. 9B). We then examined the possibility that the increased level of brain dopamine in the adult KI mice was synthesized via an alternative pathway, that is, from tyramine to dopamine. To investigate this possibility, mice were first treated with reserpine to deplete the vesicular stores of dopamine. These mice were then treated with α-MT or quinine to inhibit TH or the alternative pathway enzyme CYP2D, respectively (Bromek et al., 2011). The results revealed that brain DOPAC levels were decreased by α-MT but not by quinine in both KI and wild-type mice. These results suggested that all of the dopamine in the brains of the adult KI mice was synthesized from the classical pathway, which requires both TH and AADC.

*Compensatory regulation in KI mice*

We were interested to know if any compensatory regulation occurred in the KI mice due to chronic neurotransmitter deficiency, including the mechanism that raised the dopamine levels in adult KI mice. We first investigated adult KI mice brain gene expression. Using quantitative PCR, we quantified the amount of mRNA in the coronary brain slices containing either striatum or substantia nigra. The results revealed that the mRNA levels for DAT, VMAT2, and TH

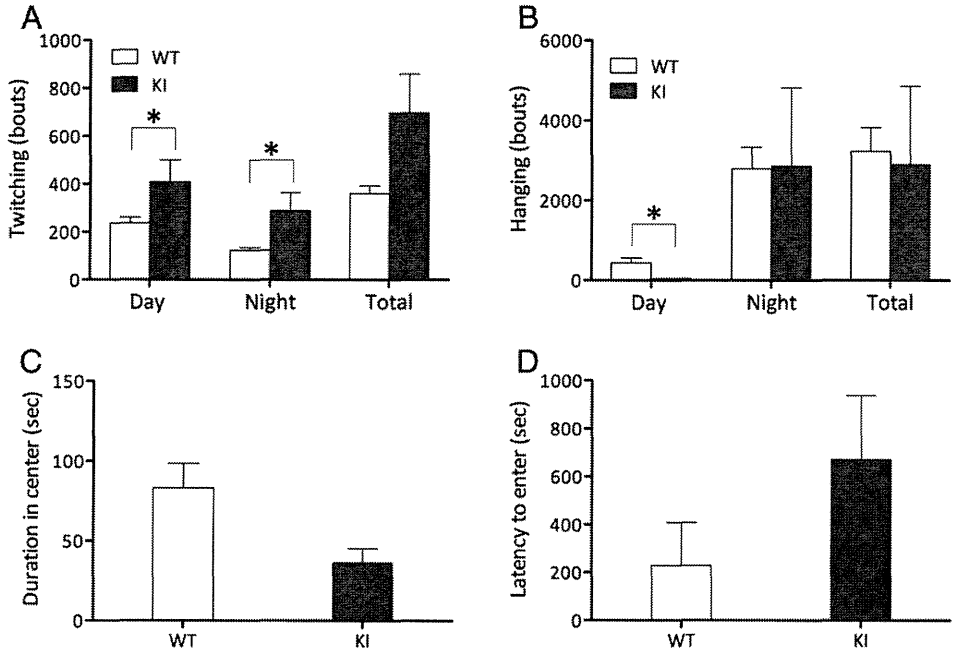


**Fig. 7.** Behavioral problems in adult (8–9 weeks of age, n = 5) KI mice. (A and B) Home-cage test. (A) The KI mice displayed more twitching than the wild-type mice ($p = 0.032$ during the day and $p = 0.008$ at night). (B) The KI mice spent less time hanging in the daytime ($p = 0.008$). (C and D) Open field test. (C) The KI mice spent less time at the center of the cage ($p = 0.076$). (D) The KI mice had a longer latency in the open field before they entered the center of the cage ($p = 0.175$). The results of the open field test did not reach statistical significance because of large individual variations. * indicates $p < 0.05$.

in the substantia nigra did not differ between the KI and wild-type mice (Fig. 10A). In the striatum, the levels of c-Fos mRNA were higher in the KI mice than in wild-type mice ($p = 0.046$), but no significant changes in the levels of COMT, and neuropeptides substance P, dynorphin, and enkephalin were observed (Fig. 10B). We further characterized mouse brain protein expression. IHC studies for the dopamine membrane transporter DAT showed similar staining patterns in both KI and wild-type mice (Figs. 10, C and D). Western blot analyses revealed no changes in the levels of dopamine receptors D1R and D2R; however, the expression of the dopamine-degrading enzyme MAOA was slightly lower in KI mice than in wild-type mice (Fig. 10F, $p = 0.05$).

Because an elevation of c-Fos gene expression may indicate increased post-synaptic neuronal excitability, we stimulated the mice

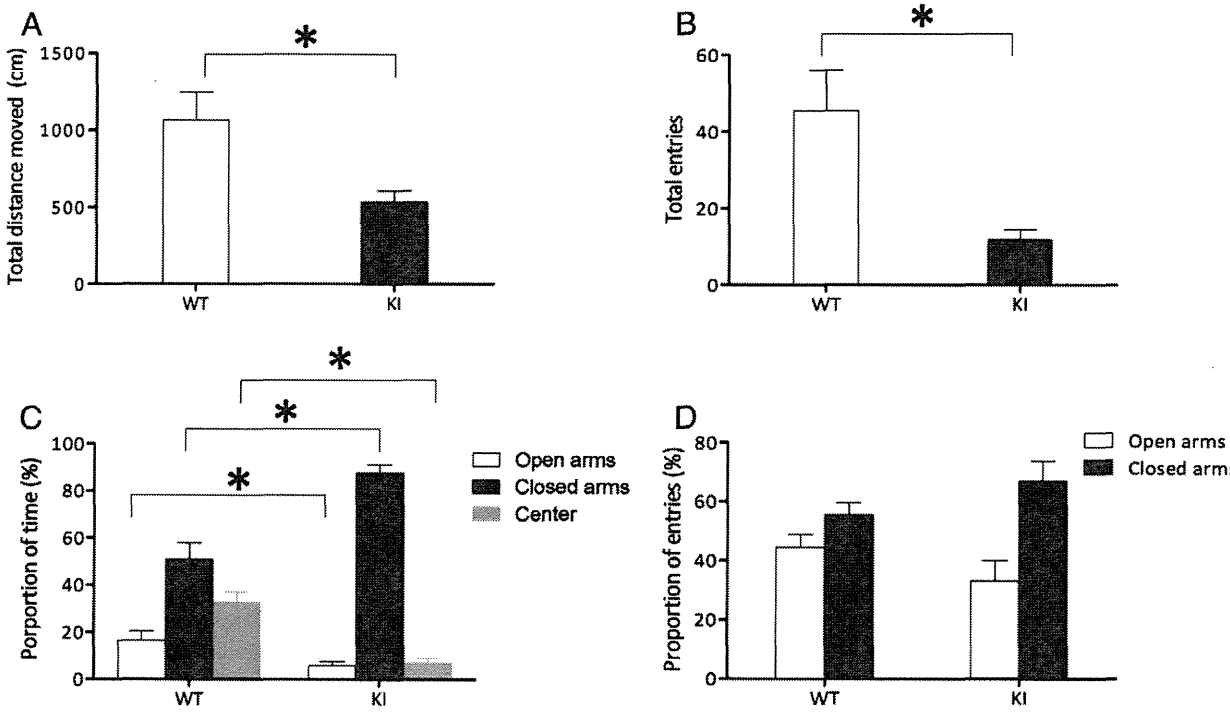


**Fig. 8.** Abnormal performance in the elevated plus maze test. (A) Total distance moved. The KI mice moved a shorter distance than the wild-type mice ($p = 0.002$). (B) Total number of arm entries. The KI mice had a lower number of entries ($p = 0.000$). (C) Proportion of time spent in each compartment. The KI mice spent more time in the closed arms ($p = 0.001$), but less time in the open arms ($p = 0.049$) or at the center ($p = 0.001$). (D) Proportion of entries into open or closed arms. * indicates $p < 0.05$.

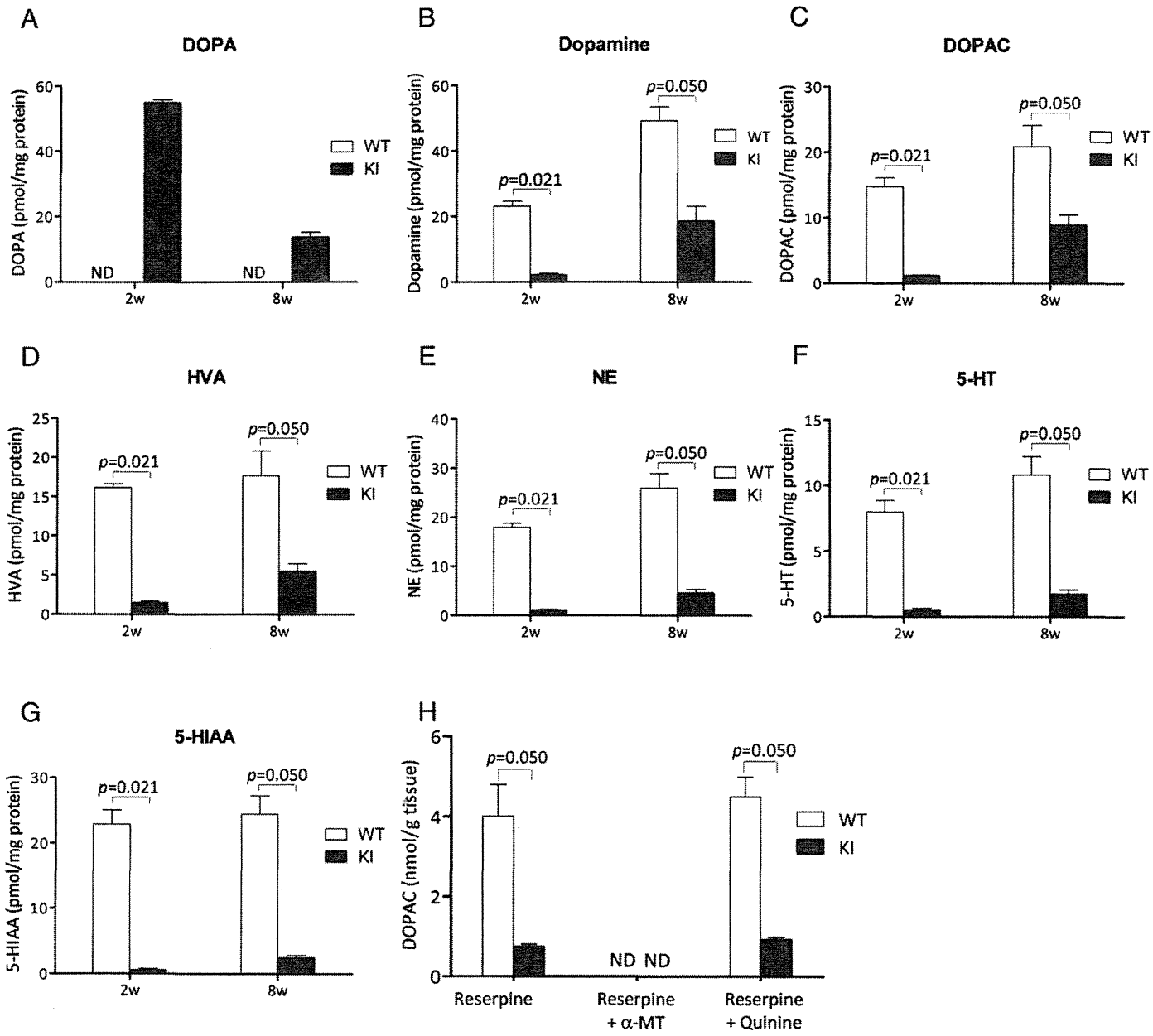


**Fig. 9.** Neurotransmitter levels in infant (2 weeks of age) and adult (8 weeks of age) KI mice brain homogenates. (A) L-DOPA (DOPA), (B) dopamine, (C) 3, 4-dihydroxyphenylacetic acid (DOPAC), (D) homovanillic acid (HVA), (E) norepinephrine (NE), (F) 5-hydroxytryptamine (5-HT, serotonin), and (G) 5-hydroxyindoleacetic acid (5-HIAA) levels. L-DOPA levels were elevated in the KI mice. All other neurotransmitters and metabolites were lower in the KI mice than in the wild-type mice, but the differences were more significant among the infantile mice than among the adult mice. (H) Dopamine production from the classical and alternative pathways. The mice were first treated with reserpine to deplete the vesicular stores of dopamine and were then treated with α-MT or quinine to inhibit TH or CYP2D, respectively. The results revealed that DOPAC levels were decreased by α-MT but not by quinine. ND: not detectable.

with the dopamine receptor agonist apomorphine. The results revealed that before apomorphine injection, the KI mice had lower total activity than the wild-type mice (Fig. 11A; $p=0.041$). After apomorphine (1.0 mg/kg) injection, the KI mice became more active (Fig. 11A; $p=0.019$) and had more rears (Fig. 11B; $p=0.001$), while the wild-type mice were suppressed. We then examined c-Fos expression 2 h after apomorphine (0.5–20 mg/kg) injection. The number of c-Fos positive nuclei increased with the dosage of apomorphine, and the KI mice revealed an exaggerated response (Fig. 11C). We then repeated the experiment with a 20-mg/kg apomorphine injection, and the difference in the number of c-Fos positive nuclei between the KI and wild-type mice was significant (Figs. 11, C and D; $p=0.004$).

## Discussion

In this study, we generated the first AADC deficiency mouse model. KI mice can survive without pharmacological or genetic rescue. The mice exhibited symptoms similar to the clinical manifestations of human AADC deficiency, including hypokinesia, dyskinesia, autonomic dysfunction, and behavioral problems. Therefore, this mouse model will be suitable for the development of gene therapies for AADC deficiency. Because patients with AADC deficiency do not respond well to pharmacological treatment, gene therapy is the optimum strategy for treating this disease. However, the current gene therapy for AADC deficiency only targets the putamen, leaving other

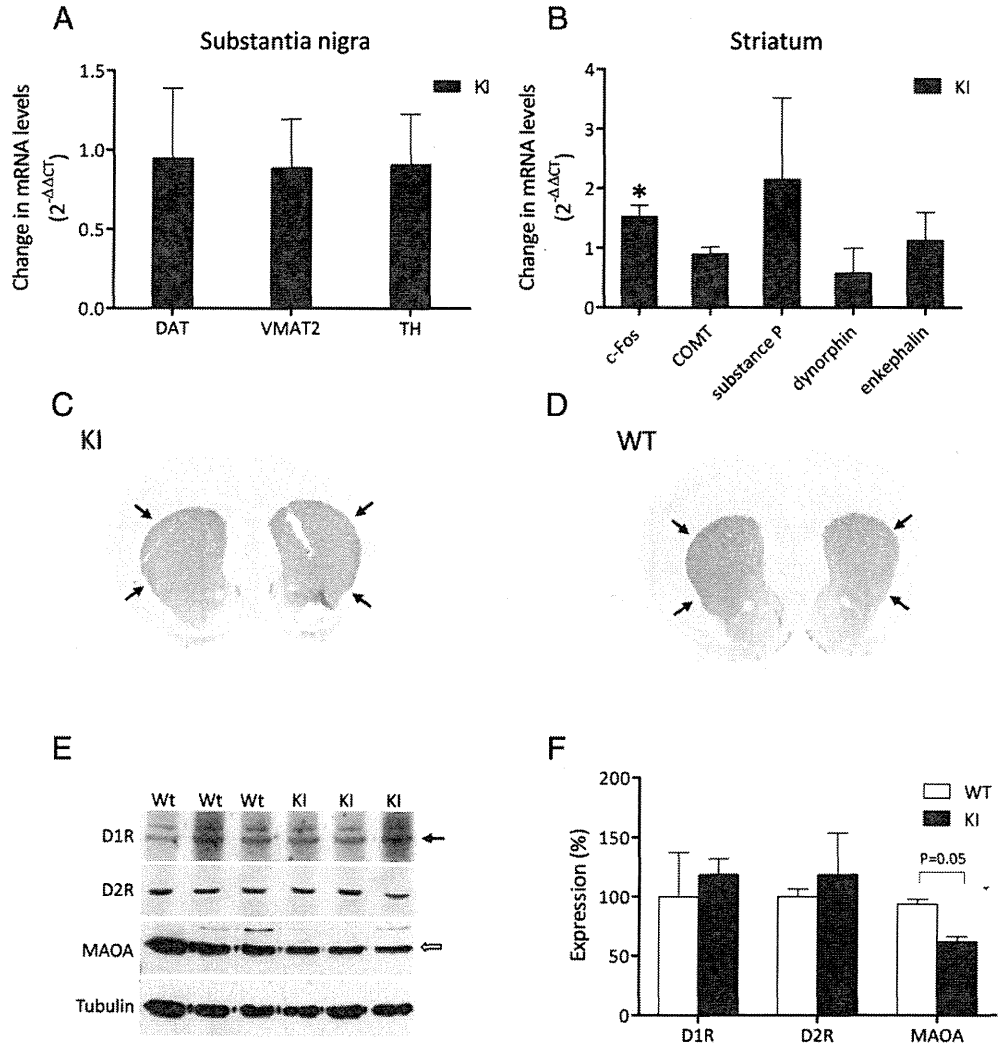


**Fig. 10.** Brain gene expression in the KI mice. (A) Quantitative PCR analyses of substantia nigra gene expression for DAT, VMAT2, and TH. Quantitative PCR results were expressed as $2^{-\Delta\Delta CT}$, representing the quantity of PCR products of KI mice relative to that of wild-type mice after normalization to the quantity of *β-actin*. No significant changes were observed. (B) Quantitative PCR analyses of striatal gene expression for c-Fos, COMT, substance P, dynorphin, and enkephalin. Only changes in c-Fos gene expression were significant ($p=0.046$). (C) Immunohistochemical staining for DAT in adult KI mice. (D) DAT staining in adult wild-type mice. No differences in DAT staining were observed between the KI and wild-type mice in the striatum (arrows). (E) Western blot analyses for the protein levels of dopamine receptor D1R (arrow) and D2R and the dopamine degrading enzyme MAOA (open arrow) in the striatum. No changes in the levels of dopamine receptors were observed, but the expression of MAOA was slightly lower in the KI mice than in the wild-type mice ($p=0.05$). (F) Quantitative results of E. * indicates $p<0.05$.

areas in the brain and body untreated (Hwu et al., 2012). The availability of an animal model is the most significant step for further development of gene therapies to treat AADC deficiency.

*Splicing errors in AADC deficiency*

The consequences of the IVS6+4A>T mutation are different between the mouse model and humans. In KI mice, this mutation leads to the skipping of exon 6. In the human AADC gene, a cryptic splicing donor at the +38 position of intron 6, which leads to a 37-nt insertion into the aberrantly spliced mRNA is observed (Lee et al., 2009). Exon 6-skipped mRNA was still detected in the lymphoblasts of patients with AADC deficiency; however, but the 37-nt insertion was the predominant mRNA species. Because the KI mice have less severe symptoms than patients with the IVS6+4A>T mutation, especially as they mature, patients can be treated by suppressing the +38 cryptic splicing site with an oligonucleotide. Splicing site suppression is currently one of the most favorable therapeutic approaches for Duchenne muscular dystrophy (Aartsma-Rus et al., 2002). Although the IVS6+4 position is conserved among most species, zebrafish possess a T rather than an A nucleotide at this position (Fig. 1A). Studying the mechanism of AADC gene splicing in zebrafish to learn how to enhance the correct splicing of the AADC gene will be interesting, as we have learned in the experimental treatment for spinal muscular atrophy (Baughan et al., 2009). Because the IVS6+4A>T mutation occurs in most Taiwanese patients with AADC deficiency, the current AADC KI mouse model will also be helpful in developing an oligonucleotide therapy.

*Residual neurotransmitter levels allow KI mice to survive*

Knocking out the genes responsible for the production of dopamine in mice usually leads to embryonic lethality or the early death of mice. Such animal models include knocking out the TH gene (Kobayashi et al., 1995; Zhou et al., 1995), or the 6-pyruvoyltetrahydropterin synthase (PTPS) (Sumi-Ichinose et al., 2001) and sepiapterin reductase (SPR)

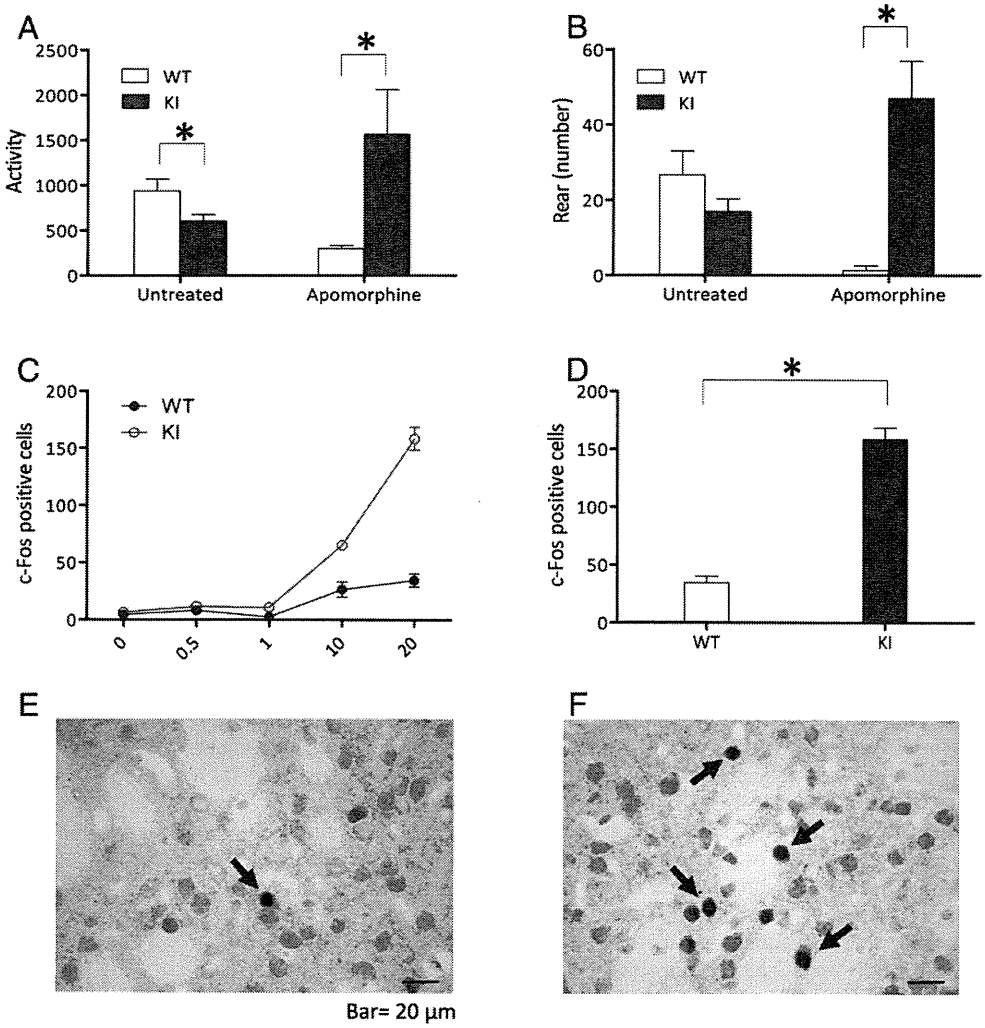


**Fig. 11.** Apomorphine stimulation test in adult mice. (A) Total activity after apomorphine stimulation. The baseline activities of the KI mice were lower than those in the wild-type mice ($p=0.041$); however, after stimulation, the activities of the KI mice were higher than those of the wild-type mice ($p=0.019$). (B) Number of rears. The baseline number of rears in the KI mice was not different from that of the wild-type mice ($p=0.272$); however, after stimulation, the number of rears in the KI mice was higher than that in the wild-type mice ($p=0.001$). (C) The mice were injected with apomorphine 0.5–20 mg/kg, and the c-Fos positive nuclei were counted in the putamen. (D) The experiment was repeated at the highest dosage that showed the greatest difference, and a quantitative result is displayed ($p=0.004$). (E) A typical c-Fos immunochemical staining image after apomorphine injection in wild-type mouse striatum, indicating that c-Fos positive cells (arrow) were rarely observed. (F) c-Fos positive cell clusters (arrows) were observed in the KI mice after apomorphine injection. * indicates $p<0.05$.

(Takazawa et al., 2008; Yang et al., 2006) genes, which are responsible for the biosynthesis of tetrahydrobiopterin ($BH_4$). These mice can be treated by L-DOPA, which effectively relieves their symptoms and allows them to survive. A genetic rescue was designed for the TH and PTPS knockout mice in which TH or PTPS is expressed in noradrenergic regions under the control of a DBH promoter (Sumi-Ichinose et al., 2005; Zhou and Palmiter, 1995). However, these treatments modified the disease and prevented the observation of the long-term outcome or chronic effects of a dopamine deficiency.

The amount of the normally spliced AADC mRNA is critical in our KI mouse model. The levels of full-length AADC mRNA in the KI mice were <0.5% of the wild-type mice levels, and the level of AADC activity was <0.3% of the wild-type mouse activity level. These levels allowed half of the homozygous embryos to be born alive and two-thirds of the live-born KI mice to survive to adulthood. Removal of the *neo* cassette from the KI mouse genome resulted in a slight increase in the levels of the normally spliced AADC mRNA but erased all the symptoms of the KI mice. These results demonstrated the difficulties in creating animal models with neurotransmitter deficiencies.

*Symptoms attributed to serotonin deficiency*

One of the limitations of the AADC deficiency model is that symptoms can arise from either dopamine or serotonin deficiency, as in models involving $BH_4$ deficiency (Sumi-Ichinose et al., 2001; Takazawa et al., 2008; Yang et al., 2006). However, if we compare our AADC KI mice with the tryptophan hydroxylase 2 (TPH2) knockout mice, which lack serotonin in the central nervous system, we can attribute some symptoms of our AADC KI mice to a serotonin deficiency (Alenina et al., 2009). The TPH2 knockout mice displayed growth retardation and 50% lethality in the first 4 weeks of postnatal life. After weaning, the TPH2 knockout mice exhibited accelerated growth and reached near-normal sizes at 4 months of age. These characteristics are similar to those observed in our AADC KI mice. Adult AADC KI mice have other symptoms in common

with TPH2 mice, including decreased blood pressure and heart rate, high anxiety, and impaired maternal care. Poor growth was also observed in TH knockout mice (Zhou and Palmiter, 1995), which suggests that dopamine deficiency affects ingestive behavior (Szczypka et al., 1999). However, increased brain dopamine levels in adult AADC KI mice coincided with the age at which serotonin deficiency no longer limits growth.

*Etiology for the spontaneous motor symptom relief in adult AADC KI mice*

A portion of AADC KI mice can survive to adulthood without intervention. Therefore, we were able to observe the natural history of the disease and found that the KI mice had fewer motor symptoms as they matured. Adult AADC KI mice displayed no dyskinesia and little hindlimb clasping, and their brain dopamine levels increased from 9.39% of the wild-type levels in infancy to 37.86% of the wild-type levels in adulthood. We considered the etiology of the increase in dopamine levels in the adult KI mice. Firstly, although AADC activity in the adult mice was still very low, AADC is not a rate-limiting enzyme and contains high basal activity; therefore, a small amount of AADC may generate a significant amount of dopamine. Secondly, brain dopamine levels normally increase with age (Fig. 9B) (Homma et al., 2011) due to an increase in the number of synapses, an increase in vesicular storage, or regulation of the recycling system (Tokuoka et al., 2011). Thirdly, we demonstrated a decrease in MAOA in the KI mice, which could lead to an increase in dopamine concentration by lower dopamine degradation.

In addition to the increased dopamine levels in the brain, postsynaptic adaptations demonstrated by the increased c-Fos levels may also contribute to the motor symptom relief in AADC KI mice. The locomotor activity response of dopamine-deficient (TH gene knockout) mice to dopamine D1 or D2 receptor agonists was exaggerated and that the acute behavioral response was correlated with c-Fos induction in the striatum (Kim et al., 2000). Moreover, trace amines and neuropeptides also modulate the dopaminergic system. Trace amines activate the trace amine-associated receptor 1 (TAAR1) and inhibit dopamine uptake by DAT (Xie et al., 2008). Because AADC mediates the syntheses of the trace amines tyramine and β-phenylethylamine (β-PEA) (Berry, 2004), the KI mice might also have a trace amine deficiency. Dopaminergic transmission stimulates striatal neuropeptide secretion (Angulo and McEwen, 1994), and neuropeptides also activate dopamine neurons in the midbrain (Kalivas, 1985). However, we did not observed any significant change in the neuropeptide mRNA levels in the KI mice. Therefore, the spontaneous symptom relief in adult KI mice is likely due to multiple factors.

*Limitations of the current study*

Currently, the etiology of spontaneous motor symptom relief in adult KI mice is not fully understood, and more studies will be necessary in the future. In the current study, we did not observe oculogyric crises in the KI mice. Oculogyric crisis is one of the most severe symptoms of AADC deficiency and occurs in most (86%) patients (Brun et al., 2010). Oculogyric crisis episodes are composed of rhythmic movements and dystonia lasting for several hours, and these episodes recur every 2–3 days. Currently, the mechanism of oculogyric crisis is unknown. An oculogyric crisis possibly occurred in the KI mice, but we were unable to recognize the symptoms. Regarding the application of this mouse model, infant KI mice displayed more symptoms but are too small for stereotactic surgery. However, the current gene therapy used in patients with AADC deficiency, which involves the stereotactic delivery of the AAV2-rAADC vector to the putamen, has achieved reasonable efficacy (Hwu et al., 2012). Therefore, future developments of gene therapies to correct AADC deficiency should focus on AAV9 or other modified AAV serotypes that can target the brain through systemic delivery. This AADC KI mouse model will be indispensable for those studies.

## Conclusion

We generated an AADC deficiency mouse model, a human disease of dopamine deficiency and motor dysfunction. Infant AADC-deficient mice displayed severe dyskinesia and poor weight gain. Adult AADC-deficient mice exhibited spontaneous motor symptom relief due to an upregulation of dopamine levels and postsynaptic excitability. This model is helpful for the development of therapies for treating dopamine deficiency.

Supplementary data to this article can be found online at http://dx.doi.org/10.1016/j.nbd.2012.12.005.

## Acknowledgments

This work was funded by a grant from the National Science Council (NSC 100-2321-B-002-041) of Taiwan and grants from the Japanese Government (a Grant-in-Aid from the Research Committee of CNS Degenerative Diseases and a Grant-in-Aid for Scientific Research on Innovative Areas "Foundations of Synapse and Neurocircuit Pathology"). The authors would like to thank the scientists from the Taiwan Mouse Clinic and the National Taiwan University Disease Animal Research Center, both of which are funded by the National Research Program for Biopharmaceuticals (NRPB). We thank the technical services provided by the "Transgenic Mouse Model Core Facility of the National Core Facility Program for Biotechnology, National Science Council" and the "Gene Knockout Mouse Core Laboratory of National Taiwan University Center of Genomic Medicine". We also thank Ms. Naomi Takino at Jichi Medical University for her help with immunohistochemistry, Mr. Hiroki Kurosaki at Tokyo Institute of Technology for his help with measuring monoamines, and Professor Jin-Chung Chen and Mr. Yueh-Ting Hsieh at Chang Gung University for their help with the dopamine receptor western blot analyses.

## References

Aartsma-Rus, A., et al., 2002. Targeted exon skipping as a potential gene correction therapy for Duchenne muscular dystrophy. Neuromuscul. Disord. 12 (Suppl. 1), S71–S77.
Abeling, N.G., et al., 1998. Aromatic L-amino acid decarboxylase deficiency: a new case with a mild clinical presentation and unexpected laboratory findings. J. Inherit. Metab. Dis. 21, 240–242.
Alenina, N., et al., 2009. Growth retardation and altered autonomic control in mice lacking brain serotonin. Proc. Natl. Acad. Sci. U. S. A. 106, 10332–10337.
Angulo, J.A., McEwen, B.S., 1994. Molecular aspects of neuropeptide regulation and function in the corpus striatum and nucleus accumbens. Brain Res. Brain Res. Rev. 19, 1–28.
Baughan, T.D., et al., 2009. Delivery of bifunctional RNAs that target an intronic repressor and increase SMN levels in an animal model of spinal muscular atrophy. Hum. Mol. Genet. 18, 1600–1611.
Benarroch, E.E., 2009. Serotonergic modulation of basal ganglia circuits: complexity and therapeutic opportunities. Neurology 73, 880–886.
Berry, M.D., 2004. Mammalian central nervous system trace amines. Pharmacologic amphetamines, physiologic neuromodulators. J. Neurochem. 90, 257–271.
Brautigam, C., et al., 2000. The influence of L-dopa on methylation capacity in aromatic L-amino acid decarboxylase deficiency: biochemical findings in two patients. J. Inherit. Metab. Dis. 23, 321–324.
Bromek, E., et al., 2011. Cytochrome P450 mediates dopamine formation in the brain in vivo. J. Neurochem. 118, 806–815.
Brun, L., et al., 2010. Clinical and biochemical features of aromatic L-amino acid decarboxylase deficiency. Neurology 75, 64–71.
Bruneau, G., et al., 1992. Mapping of the dopa decarboxylase gene to the 11A band of the murine genome. Biochem. Biophys. Res. Commun. 186, 926–930.
Consortium, T. U., 2011. Ongoing and future developments at the Universal Protein Resource. Nucleic Acids Res. 39, D214–D219.
Crittenden, J.R., Graybiel, A.M., 2011. Basal ganglia disorders associated with imbalances in the striatal striosome and matrix compartments. Front Neuroanat. 5, 59.
Fiumara, A., et al., 2002. Aromatic L-amino acid decarboxylase deficiency with hyperdopaminuria. Clinical and laboratory findings in response to different therapies. Neuropediatrics 33, 203–208.
Gantois, I., et al., 2007. Ablation of D1 dopamine receptor-expressing cells generates mice with seizures, dystonia, hyperactivity, and impaired oral behavior. Proc. Natl. Acad. Sci. U. S. A. 104, 4182–4187.
Hamosh, A., McKusick, V. A., DOPA decarboxylase; DDC. Johns Hopkins University, OMIM® database 2011.
Homma, D., et al., 2011. Partial biopterin deficiency disturbs postnatal development of the dopaminergic system in the brain. J. Biol. Chem. 286, 1445–1452.

Hwu, W.L., et al., 2012. Gene therapy for aromatic L-amino acid decarboxylase deficiency. Sci. Transl. Med. 4, 134ra61.
Hyland, K., Clayton, P.T., 1990. Aromatic amino acid decarboxylase deficiency in twins. J. Inherit. Metab. Dis. 13, 301–304.
Hyland, K., et al., 1992. Aromatic L-amino acid decarboxylase deficiency: clinical features, diagnosis, and treatment of a new inborn error of neurotransmitter amine synthesis. Neurology 42, 1980–1988.
Ichinose, H., et al., 1985. Simple purification of aromatic L-amino acid decarboxylase from human pheochromocytoma using high-performance liquid chromatography. Anal. Biochem. 150, 408–414.
Kalivas, P.W., 1985. Interactions between neuropeptides and dopamine neurons in the ventromedial mesencephalon. Neurosci. Biobehav. Rev. 9, 573–587.
Kim, D.S., et al., 2000. Dopamine-deficient mice are hypersensitive to dopamine receptor agonists. J. Neurosci. 20, 4405–4413.
Kobayashi, K., et al., 1995. Targeted disruption of the tyrosine hydroxylase locus results in severe catecholamine depletion and perinatal lethality in mice. J. Biol. Chem. 270, 27235–27243.
Korenke, G.C., et al., 1997. Aromatic L-amino acid decarboxylase deficiency: an extrapyramidal movement disorder with oculogyric crises. Eur. J. Paediatr. Neurol. 1, 67–71.
Lee, H.F., et al., 2009. Aromatic L-amino acid decarboxylase deficiency in Taiwan. Eur. J. Paediatr. Neurol. 13, 135–140.
Lin, C.J., et al., 2010. Cellular localization of the organic cation transporters, OCT1 and OCT2, in brain microvessel endothelial cells and its implication for MPTP transport across the blood–brain barrier and MPTP-induced dopaminergic toxicity in rodents. J. Neurochem. 114, 717–727.
Liu, P., et al., 2003. A highly efficient recombineering-based method for generating conditional knockout mutations. Genome Res. 13, 476–484.
Livak, K.J., Schmittgen, T.D., 2001. Analysis of relative gene expression data using real-time quantitative PCR and the 2(−Delta Delta C(T)) Method. Methods 25, 402–408.
Maller, A., et al., 1997. Aromatic L-amino acid decarboxylase deficiency: clinical features, diagnosis, and treatment of a second family. J. Child Neurol. 12, 349–354.
Nagatsu, I., et al., 1979. Immunocytochemical localization of tyrosine hydroxylase, dopamine-beta-hydroxylase and phenylethanolamine-N-methyltransferase in the adrenal glands of the frog and rat by a peroxidase-antiperoxidase method. Histochemistry 64, 131–144.
Nagatsu, I., et al., 1988. Aromatic L-amino acid decarboxylase-immunoreactive neurons in and around the cerebrospinal fluid-contacting neurons of the central canal do not contain dopamine or serotonin in the mouse and rat spinal cord. Brain Res. 475, 91–102.
Pons, R., et al., 2004. Aromatic L-amino acid decarboxylase deficiency: clinical features, treatment, and prognosis. Neurology 62, 1058–1065.
Rozas, G., et al., 1997. An automated rotarod method for quantitative drug-free evaluation of overall motor deficits in rat models of parkinsonism. Brain Res. Brain Res. Protoc. 2, 75–84.
Su, K.Y., et al., 2007. Mice deficient in collapsin response mediator protein-1 exhibit impaired long-term potentiation and impaired spatial learning and memory. J. Neurosci. 27, 2513–2524.
Sumi-Ichinose, C., et al., 1992. Molecular cloning of genomic DNA and chromosomal assignment of the gene for human aromatic L-amino acid decarboxylase, the enzyme for catecholamine and serotonin biosynthesis. Biochemistry 31, 2229–2238.
Sumi-Ichinose, C., et al., 2001. Catecholamines and serotonin are differently regulated by tetrahydrobiopterin. A study from 6-pyruvoyltetrahydropterin synthase knockout mice. J. Biol. Chem. 276, 41150–41160.
Sumi-Ichinose, C., et al., 2005. Genetically rescued tetrahydrobiopterin-depleted mice survive with hyperphenylalaninemia and region-specific monoaminergic abnormalities. J. Neurochem. 95, 703–714.
Swoap, S.J., et al., 2004. Dbh(−/−) mice are hypotensive, have altered circadian rhythms, and have abnormal responses to dieting and stress. Am. J. Physiol. Regul. Integr. Comp. Physiol. 286, R108–R113.
Swoboda, K.J., et al., 1999. Clinical and therapeutic observations in aromatic L-amino acid decarboxylase deficiency. Neurology 53, 1205–1211.
Swoboda, K.J., et al., 2003. Aromatic L-amino acid decarboxylase deficiency: overview of clinical features and outcomes. Ann. Neurol. 54 (Suppl. 6), S49–S55.
Szczypka, M.S., et al., 1999. Feeding behavior in dopamine-deficient mice. Proc. Natl. Acad. Sci. U. S. A. 96, 12138–12143.
Takazawa, C., et al., 2008. A brain-specific decrease of the tyrosine hydroxylase protein in sepiapterin reductase-null mice—as a mouse model for Parkinson's disease. Biochem. Biophys. Res. Commun. 367, 787–792.
Tay, S.K., et al., 2007. Unusually mild phenotype of AADC deficiency in 2 siblings. Mol. Genet. Metab. 91, 374–378.
Tokuoka, H., et al., 2011. Compensatory regulation of dopamine after ablation of the tyrosine hydroxylase gene in the nigrostriatal projection. J. Biol. Chem. 286, 43549–43558.
Vuckovic, M.G., et al., 2010. Exercise elevates dopamine D2 receptor in a mouse model of Parkinson's disease: in vivo imaging with [(1)F]fallypride. Mov. Disord. 25, 2777–2784.
Wu, W.L., et al., 2010. Mice lacking Asic3 show reduced anxiety-like behavior on the elevated plus maze and reduced aggression. Genes Brain Behav. 9, 603–614.
Xie, Z., et al., 2008. Modulation of monoamine transporters by common biogenic amines via trace amine-associated receptor 1 and monoamine autoreceptors in human embryonic kidney 293 cells and brain synaptosomes. J. Pharmacol. Exp. Ther. 325, 629–640.
Yang, S., et al., 2006. A murine model for human sepiapterin-reductase deficiency. Am. J. Hum. Genet. 78, 575–587.
Zhou, Q.Y., Palmiter, R.D., 1995. Dopamine-deficient mice are severely hypoactive, adipsic, and aphagic. Cell 83, 1197–1209.
Zhou, Q.Y., et al., 1995. Targeted disruption of the tyrosine hydroxylase gene reveals that catecholamines are required for mouse fetal development. Nature 374, 640–643.

*International Journal of Neuropsychopharmacology*, Page 1 of 9. © CINP 2013
doi:10.1017/S1461145712001575

ARTICLE

# Intrastriatal gene delivery of GDNF persistently attenuates methamphetamine self-administration and relapse in mice

**Yijin Yan[1,2], Yoshiaki Miyamoto[3], Atsumi Nitta[3], Shin-ichi Muramatsu[4], Keiya Ozawa[5], Kiyofumi Yamada[1] and Toshitaka Nabeshima[1,6,7,8]**

[1] *Department of Neuropsychopharmacology and Hospital Pharmacy, Nagoya University Graduate School of Medicine, Nagoya, Japan*
[2] *Department of Anesthesia and Critical Care, The University of Chicago, Chicago, IL, USA*
[3] *Department of Pharmaceutical Therapy and Neuropharmacology, Faculty of Pharmaceutical Sciences, Graduate School of Medicine and Pharmaceutical Sciences, University of Toyama, Toyama, Japan*
[4] *Division of Neurology, Department of Medicine, Jichi Medical University, Shimotsuke, Japan*
[5] *Division of Genetic Therapeutics, Center for Molecular Medicine, Jichi Medical University, Shimotsuke, Japan*
[6] *Department of Chemical Pharmacology, Graduate School of Pharmaceutical Sciences, Meijo University, Nagoya, Japan*
[7] *Japanese Drug Organization of Appropriate Drug Use and Research, Nagoya, Japan*
[8] *Department of Regional Pharmaceutical Care and Sciences, Meijo University, 150 Yagotoyama, Nagoya, Japan*

**Abstract**

Relapse of drug abuse after abstinence is a major challenge to the treatment of addicts. In our well-established mouse models of methamphetamine (Meth) self-administration and reinstatement, bilateral microinjection of adeno-associated virus vectors expressing GDNF (AAV-Gdnf) into the striatum significantly reduced Meth self-administration, without affecting locomotor activity. Moreover, the intrastriatal AAV-Gdnf attenuated cue-induced reinstatement of Meth-seeking behaviour in a sustainable manner. In addition, this manipulation showed that Meth-primed reinstatement of Meth-seeking behaviour was reduced. These findings suggest that the AAV vector-mediated Gdnf gene transfer into the striatum is an effective and sustainable approach to attenuate Meth self-administration and Meth-associated cue-induced relapsing behaviour and that the AAV-mediated Gdnf gene transfer in the brain may be a valuable gene therapy against drug dependence and protracted relapse in clinical settings.

*Received 16 August 2012; Reviewed 29 August 2012; Revised 26 November 2012; Accepted 1 December 2012*

**Key words**: Adeno-associated virus, cue-induced reinstatement, gene therapy, glial cell line-derived neurotrophic factor, methamphetamine, self-administration.

## Introduction

Glial cell line-derived neurotrophic factor (GDNF) has been widely tested as a potential therapeutic agent for the treatment of Parkinson's disease (Tomac et al., 1995; Choi-Lundberg et al., 1997; Mandel et al., 1997; Kordower et al., 2000; Wang et al., 2002; Kirik et al., 2004), since GDNF was originally purified from a rat glioma cell-line supernatant as a trophic factor for embryonic midbrain dopamine neurons (Lin et al., 1993). Dopaminergic transmission from the ventral tegmental area to nucleus accumbens and prefrontal cortex plays an important role in the development of drug addiction and striatal dopaminergic transmission is critical for the conversion from drug use to drug abuse or habit formation (Everitt and Robbins, 2005; Di Ciano et al., 2008). Therefore, it is reasonable to postulate that GDNF may be involved in the development of drug addiction (Pierce and Bari, 2001). Indeed, GDNF has been identified as a critical modulator in the development of drug dependence in animal models (Messer et al., 2000; He et al., 2005; Niwa et al., 2007a, b; Lu et al., 2009). The manipulations that increase contents of GDNF in the striatum and nucleus accumbens attenuate acquisition of cocaine self-administration in rats (Green-Sadan et al., 2003, 2005). In contrast, the manipulations that decrease contents of GDNF in the brain facilitate drug-induced conditioned place preference and drug self-administration in rodent animals (Messer et al., 2000; Niwa et al., 2007a, b; Yan et al., 2007b). Previously, we have reported that a reduction of endogenous GDNF protein in heterozygous GDNF knockout mice ($GDNF^{+/-}$ mice) not only facilitates the acquisition of methamphetamine (Meth) self-administration, results in an upward shift in the dose–response curve and increases

Address for correspondence: Professor T. Nabeshima, Department of Regional Pharmaceutical Care and Sciences, Graduate School of Pharmaceutical Sciences, Meijo University, Nagoya 468-8503, Japan.
*Tel.*: +81 52 839 2756 *Fax*: +81 52 839 2756
*Email*: tnabeshi@meijo-u.ac.jp

motivation to take Meth, but also leads to increased vulnerability to Meth-primed reinstatement and enduring vulnerability to cue-induced relapsing behaviour (Yan et al., 2007b). In a clinical setting, GDNF itself cannot be orally administered for the treatment of brain diseases. The next challenge we had was to investigate safe and permanent potentiation of GDNF expression only in the critical local brain areas. Adeno-associated viral (AAV) vector is one of the most useful tools for the delivery of therapeutic genes into the brain as a potential therapeutic strategy against brain diseases, because of its safety and sustainable expression in the dopaminergic transmission pathways in the brain (Wang et al., 2002; Eberling et al., 2009; Su et al., 2009). In aged rats or Parkinsonian non-human primates, AAV-Gdnf-treated animals show clinical improvement and functional recovery in the nigrostriatal pathway without adverse effects (Eberling et al., 2009; Johnston et al., 2009; Kells et al., 2010). Recently, we used the AAV vector as a vehicle of the aromatic L-amino acid decarboxylase gene into the putamen of Parkinson's disease patients for a clinical phase I study (Muramatsu et al., 2010). In this study, we determine effects of an intrastriatal microinjection of the AAV-Gdnf on Meth self-administration, extinction and reinstatement of Meth-seeking behaviour in mice.

## Materials and method

### *Subjects and drugs*

Male C57BL/6J mice were aged 8 wk and weighed 20–25 g at the beginning of the experiments. They were kept in a regulated environment ($23 \pm 0.5$ °C; $50 \pm 0.5$% humidity) with a 12-h light/dark cycle (lights on 09:00 hours). Water and food were available *ad libitum*. To minimize the number of animals in the experiments, a within-subjects design was used in Meth self-administration, extinction and reinstatement of Meth-seeking behaviour induced by either Meth-priming injection or presentation of Meth-associated cues in our experiments. All procedures followed the National Institute of Health Guidelines for the Care and Use of Laboratory Animals and were approved by the Nagoya University Animal Care and Use Committee.

Meth hydrochloride (Dainippon Pharmaceutical Ltd, Japan) was dissolved in sterile saline and self-administered at a dose of 0.1 mg/kg.infusion over 5 s (infusion volume 2.1 $\mu$l; Yan et al., 2006, 2007a).

### *The AAV vectors expressing GDNF*

The AAV-Gdnf or AAV-EGFP was constructed and prepared as previously described (Wang et al., 2002). In the present study, the final particle titre for the intrastriatal microinjection of the AAV-Gdnf and AAV-EGFP was $8.4 \times 10^{13}$ and $6.4 \times 10^{13}$ vector genome copies/ml, respectively.

### *Surgery for intravenous implantation of catheter and bilateral intrastriatal injection of the AAV-Gdnf*

#### *Catheter implantation for Meth infusion*

Naive mice were anaesthetized with pentobarbital sodium (50 mg/kg i.p.). Indwelling catheters were constructed of micro-silicone tubing (inner diameter, 0.50 mm; outer diameter, 0.7 mm; Imamura Co., Ltd, Japan) and polyethylene tubing (inner diameter, 0.50 mm; outer diameter, 0.8 mm). Incisions were made on the skin of the head and ventral neck and the right jugular vein was externalized. The end of the catheter was inserted into the jugular vein via a small incision and was secured to the vein and surrounding tissue with silk sutures. The exit port of the catheter passed subcutaneously to the top of the skull and was temporarily closed with a clamp.

#### *Bilateral intrastriatal microinjection of the AAV-Gdnf and AAV-EGFP vectors*

Once the intravenous was successfully implanted as described above, the animals received bilateral microinjection of the AAV vectors into the striatum, according to the standard mouse brain coordinates (Franklin and Paxinos, 2007). Based on previous reports (Tomac et al., 1995; Chen et al., 2008), the AAV-Gdnf or AAV-EGFP vectors were bilaterally injected into the striatum ($+0.9$ mm anteroposterior, $\pm 1.5$ mm mediolateral, $-3.0$ and $-2.0$ mm dorsoventral) at two different depths through a 10 $\mu$l Hamilton syringe (Hamilton Company, USA) with a 33 gauge blunt hypodermic needle. At a lower site, the vectors were bilaterally injected in a volume of 1.0 $\mu$l/site over 2 min and the syringe needle was left in place for an additional 3 min. After the needle was pulled upward 1.0 mm (upper site), the vectors were bilaterally injected in a volume of 1.0 $\mu$l/site over 2 min and an additional 3 min for the needle in place. The burr hole was sealed with quick self-curing acrylic resin (Shofu Inc., Japan) after each injection.

### *Measurement of motility in a novel environment*

Motility in a novel environment was measured in a transparent acrylic cage with a black Plexiglas floor ($45 \times 45 \times 40$ cm) using infrared counters (Scanet SV-40; MELQUEST, Japan). Two weeks after recovering from the bilateral intrastriatal microinjection of the AAV-Gdnf or AAV-EGFP vectors, the two groups of mice (AAV-Gdnf and AAV-EGFP) were placed in the centre of the cage and allowed to move freely for 60 min. Locomotion and rearing were analysed to examine effects of the intrastriatal microinjection of the AAV-Gdnf or AAV-EGFP vector on motility in general in mice.

### *Immunohistochemical staining for GDNF*

Brain sections (16 $\mu$M) were cut on a cryostat, thaw-mounted on Silane-coated slides and stored at $-80$ °C